Mathematical and Statistical Sciences Faculty Publications and Presentations

College of Sciences

10-30-2022

Study of Multilayer Flow of a Bi-Viscous Bingham Fluid Sandwiched Between Hybrid Nanofluid in a Vertical Slab with Nonlinear Boussinesq Approximation

Mahanthesh Basavarajappa
The University of Texas Rio Grande Valley, mahanthesh.b@utrgv.edu

Shruthy Myson

Kuppalapalle Vajravelu

Recommended Citation

Mahanthesh Basavarajappa , Shruthy Myson , and Kuppalapalle Vajravelu , "Study of Multilayer Flow of a Bi-Viscous Bingham Fluid Sandwiched Between Hybrid Nanofluid in a Vertical Slab with Nonlinear Boussinesq Approximation", Physics of Fluids (in press) (2022); https://doi.org/10.1063/5.0123131

Study of Multilayer Flow of a Bi-Viscous Bingham Fluid Sandwiched Between Hybrid Nanofluid in a Vertical Slab with Nonlinear Boussinesq Approximation

ID Mahanthesh Basavarajappa, ID Shruthy Myson and ID Kuppalapalle Vajravelu

View Online   Export Citation   CrossMark

ARTICLES YOU MAY BE INTERESTED IN

Control and suppression of viscous fingering displacing non-Newtonian fluid with time-dependent injection strategies
Physics of Fluids **34**, 114117 (2022); https://doi.org/10.1063/5.0124066
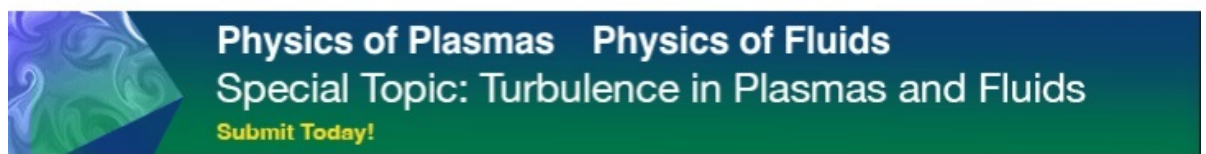
Migration dynamics of an initially spherical deformable bubble in the vicinity of a corner
Physics of Fluids **34**, 112119 (2022); https://doi.org/10.1063/5.0115162

Study of flow of Buongiorno nanofluid in a conical gap between a cone and a disk
Physics of Fluids **34**, 112004 (2022); https://doi.org/10.1063/5.0121642

AIP Publishing

Study of Multilayer Flow of a Bi-Viscous Bingham Fluid Sandwiched Between Hybrid Nanofluid in a Vertical Slab with Nonlinear Boussinesq Approximation

Mahanthesh Basavarajappa[1,*], Shruthy Myson[2], and Kuppalapalle Vajravelu[3]

[1]School of Mathematical and Statistical Sciences, The University of Texas Rio Grande Valley, Edinburg, TX 78531, USA.

[2]Center for Mathematical Needs, Department of Mathematics, CHRIST (Deemed to be University), Bengaluru-560029, Karnataka, INDIA.

[3]Department of Mathematics, Department of Mechanical, Material and Aerospace Engineering, University of Central Florida, Orlando, FL32816, USA

*Corresponding Author Email: mahanthesh.b@utrgv.edu

Abstract: Bi-Viscosity Bingham plastic fluids are used to understand the rheological characteristics of pigment-oil suspensions, polymeric gels, emulsions, heavy oil, etc. High-temperature applications in many industrial and engineering problems, linear density-temperature variation is inadequate to describe convective heat transport. Therefore, the characteristics of the nonlinear convective flow of a Bi-Viscosity Bingham Fluid (BVBF) through three layers in a vertical slab are studied. The two outer layers of the oil-based hybrid nanofluid and the intermediate layer of BVBF are considered. The thermal buoyancy force is governed by the nonlinear Boussinesq approximation. Continuity of heat flux, velocity, shear stress, and temperature are imposed on the interfaces. The governing equations are derived from the Navier-Stokes equation, conservation of energy, and conservation of mass for three layers. The nonlinear multipoint (four-point) boundary value problem (NMBVP) is solved using the differential transform method (DTM). Converging DTM solutions are obtained, and they are validated. The entropy equation and Bejan number were also derived and analyzed. It is established that the nonlinear density-temperature variation leads to a significant improvement in the magnitude of the velocity and temperature profiles due to the increased buoyancy force and as a result, the drag force on the walls is reduced. The drag force on the slab gets reduced by decreasing the volume of nanoparticles. Furthermore, nonlinear convection and mixed convection give rise to an advanced rate of heat transport on the walls and thereby to an enhanced heat transport situation.

Keywords: Multilayer flow; Vertical slab; Hybrid nanoliquid; Nonlinear Boussinesq approximation; Entropy generation; Differential transform method.

I. INTRODUCTION

Yield stress fluids demonstrate a stress threshold that separates different fluid behaviors. Flow occurs when the yield point is exceeded; otherwise, the fluid behaves like a solid. Several real-world fluids, such as pigment-oil suspensions, polymer gels, emulsions, heavy oils, biopolymers, pastes, foams, etc., possess these characteristics. These fluids are used in polymer industries, petroleum recovery, petroleum extraction, and food processing applications[1]. Bingham model[2] exhibits the linear relationship between shear stress and shear rate beyond yield stress. However, the apparent viscosity diverges due to zero velocity gradient[3]. To overcome this, the regularization of the Bingham fluid model was made by Nakamura and Sawada[4] and proposed a Bi-Viscous Bingham fluid (BVBF) model (mostly reported as Casson fluid in the literature). They compared their rheological features with the Casson fluid model[5] and showed that BVBF and the Casson fluid models have negligible differences since these two constitutive models resemble each other except in the region of modest shear rate. Dandapat *et al[6]* studied the bi-viscosity fluid flow problem analytically by considering a thin liquid film on extending surface. Hayat *et al.*[7] studied the flow of Casson liquid with the magnetic field, Soret, and Dufour effects on a stretched surface. They showed that the Casson parameter has a diminishing effect on the velocity and an opposite effect on temperature distribution. Reddy *et al*[8] examined the significance of Joule heating, Soret, and Hall effects on Casson liquid in a vertical slab. [9]Kumar and Mondal studied the buoyancy-driven transport of Casson fluid over a wavy plate using the Crank-Nicolson technique. Recently, Frigaard and Poole[10] commented that the constitutive relationship considered in the studies[7-9], the suitable way to name the fluid would be bi-viscous Bingham fluid (BVBF) instead of Casson. Because of the applications and relevance, the current study deals with the BVBF multilayer flow in a vertical slab.

The *nanoliquid* concept was initiated by Choi and Eastman[11] to improve the efficiency of heat transfer in working liquids. Typical working liquids with lower thermal conductivity (such as oil, water, and ethylene glycol) have inadequate heat transport capacity. To improve the heat transport characteristics, working liquids and nanoparticles are suspended to create a composition with higher thermal conductivity. This suspension is called *nanoliquid*. There are three different nanofluid models available to theoretically study the convective heat transfer in nanoliquids. Namely, the single-phase model (KVL model), the inhomogeneous two-component model (Buongiorno model), and the modified Buongiorno model. The KVL model[12] is based on the same relative velocity of the base fluid and the nanoparticles. Due to

the nanometer size of the particles, they can be liquefied and then treated as a single-phase liquid rather than a fluid-particle suspension. In this study, we consider a single-phase model to describe the nanofluid flow by employing effective nanofluid properties.

Although nanoliquids address the deficiency of low thermal conductivity, further research in this field has helped to develop a new class of liquids known as *composite nanoliquids*, which have a higher thermal efficiency than *mono nanoliquids*. Composite nanoliquids are made by mixing two or more different types of nanoparticles. They have superior physical and chemical properties, which is not the case with mono nanoliquids. Hybrid nanoliquids also aim to improve the stability of the system. The term stability is used to define the performance and thermal efficiency of nanoliquids over time. To achieve better stability and improved heat transport capability, copper-alumina (1% of Cu + 3% of Al_2O_3) nanoparticles are chosen for the study. Suresh et al.[13] experimentally analyzed the heat transfer in $Al_2O_3 - Cu$/water hybrid nanoliquids and established that hybrid nanoliquids have greater heat transfer enhancement than mono nanoliquids. An elevated average Nusselt number situation occurred due to the use of $Cu - Al_2O_3$ water hybrid nanoliquid. Some studies relating to hybrid nanoliquids can be seen in[14-20].

Multilayer flow of immiscible fluids is of great interest in various applications related to the polymer industry, petroleum industry, oil extraction, food processing, etc. Multilayer transport of fluids reduces the pumping power required to pump oil into a pipeline by adding an adequate amount of water. Especially in the polymer industry, multilayer films are produced by coextrusion and are used as products with advanced physical and optical properties. Each layer of these composite materials offers a certain end-use characteristic, such as mechanical and thermoforming properties. Applications for multilayer films range from food packaging to laminated paper. Several other applications of the multilayer flows are highlighted in the studies[21-26]. Packham and Shall[21] discussed the laminar flow of two non-miscible liquids by taking a horizontal tube. They found that the flow rate is greater in a multi-layer system than in a single-layer system. Umavathi and Malashetty[22] presented a study of multilayer flow in a vertical slab with viscous and magnetic effects. The velocity and temperature are calculated for both symmetric and asymmetric heating. Vajravelu *et al.*[23] analyzed the heat transmission of nanoliquids in a multilayer stream and showed that increasing the concentration of the nanoparticle in the base liquid changes the velocity of the liquid at the interface and reduces the shear stress, both, at the interface and the surface of the slab. Li *et al.*[24] considered the mixed convection flow in a two-layer vertical slab, where the first layer is filled with

3

nanoliquid, and the second layer is filled with a power-law liquid. Some of the recent works in this area are Sarma *et al.*[25], and Umavathi and Bég[26].

Joseph Valentin Boussinesq introduced the concept of the Boussinesq approximation which states that density is considered constant throughout the momentum equation until gravity is multiplied. In the above studies, the density-temperature relationship is assumed to be linear. However, the density does not vary linearly due to temperature/concentration/ pressure when the temperature difference is relatively large in the system. Furthermore, the non-linear variation of density and temperature significantly affects the fluid system and therefore cannot be ignored. Goren[27] studied the nonlinear density variation with temperature in water. Few other prominent early works related to nonlinear Boussinesq approximation (NBA) can be seen in[28,29]. Partha[30] investigated the impact of nonlinear Boussinesq approximation (NBA) in a porous medium. Shaw *et al.*[31] analyzed the behavior of BVBF with nonlinear convection in the presence of suction/injection, Soret, and Dufour effects. Naveen and Reddy[32] scrutinized the effects of viscous dissipation and the chemical reaction on nonlinear convective heat transfer in a Casson liquid. Besides, the Rosseland approximation is generally used to study the effects of thermal radiation. The Rosseland approximation demands an optically dense medium with radiation that travels only a short distance before scattering or absorption. Some of the recent concerning the nonlinear Boussinesq approximation and thermal radiation are in[33-35]. However, the studies on the application of nonlinear Boussinesq approximation in multilayer flow with thermal radiation effect are very limited.

The literature does not encompass a study of heat transfer in a BVBF sandwiched between hybrid nanoliquids in a vertical slab with a nonlinear density-temperature variation. The effects of thermal radiation and viscous dissipation are taken into account in the thermal energy equation. The entropy generation analysis is also performed because, as we are dealing with two-layer hybrid nanofluids, there would be a trade-off. Hybrid nanofluids improve the heat transport situation in the system, at the same time, due to the increase in viscosity, the necessary pumping power would be penalized. Entropy production analysis enables us to determine the effectiveness because it considers both heat transport and fluid friction irreversibility. Further details of entropy generation analysis can be found in[36-41]. The middle region is filled with BVBF, and the outer regions are filled with oil-based $Cu - Al_2O_3$ hybrid nanoliquid. Semi-analytical Differential Transform Method (DTM) is employed to solve the multi-point boundary value problem.

II.   MATHEMATICAL FORMULATION

A.   The Constitutive Equation and Rosseland Approximation

The stress-tensor of the BVBF[4] in subscript form is given below:

$$
\tau_{ij} =
\begin{cases}
2\left(\mu_B + \dfrac{p_y}{\sqrt{2\Pi}}\right)e_{ij}, & \Pi \geq \Pi_c \\[2mm]
2\left(\mu_B + \dfrac{p_y}{\sqrt{2\Pi_c}}\right)e_{ij}, & \Pi < \Pi_c
\end{cases}
\tag{1}
$$

where τ_{ij} is the Cauchy stress-tensor, μ_B is the plastic dynamic viscosity, p_y is the yield stress, e_{ij} is the $(i,j)^{th}$ component of deformation rate, $\Pi = e_{ij}e_{ij}$ is the product of deformation tensor with itself, and Π_c is the critical value of Π. The dimensionless BVBF parameter is given below:

$$
\gamma = \frac{\mu_B\sqrt{2\Pi_c}}{p_y}\,.
\tag{2}
$$

The comprehensive study of regularized Bingham fluid model was made by Nakamura and Sawada[4], and its rheological features are compared with the Casson fluid model. They showed that regularized (bi-viscous) Bingham and the Casson fluid models have insignificant differences as these two constitutive models resemble each other except in the modest shear rate region. However, the regularized (bi-viscous) Bingham fluid possesses high yield stress in comparison to the Casson model.

The Rosseland approximation depends on the theory that the fluid (medium) is optically thick. If the reciprocal of the elimination/absorption factor is negligibly small compared to the characteristic dimension of the medium, a medium is said to be optically thick. The net radiative heat flux ($\boldsymbol{q_{ri}}$) using well-known Rosseland approximation is given below[35]:

$$
\boldsymbol{q_{ri}} = -\frac{4}{3a_R}\nabla e_b\,,
\tag{3}
$$

where a_R is the Rosseland mean absorption factor and e_b is blackbody emissive power. Using the Stefan-Boltzmann radiation law:

$$
e_b = \sigma_{SB}T_i^4\,,
\tag{4}
$$

here σ_{SB} is the Stefan-Boltzmann constant, T is the temperature, and in T_i and $\boldsymbol{q_{ri}}$, the subscript i $(i = 1,2,3)$ used to represent the regions I, II, and III correspondingly. Using Eq. (4),

$$
\boldsymbol{q_{ri}} = -\frac{4\sigma_{SB}}{3a_R}\nabla T_i^4\,.
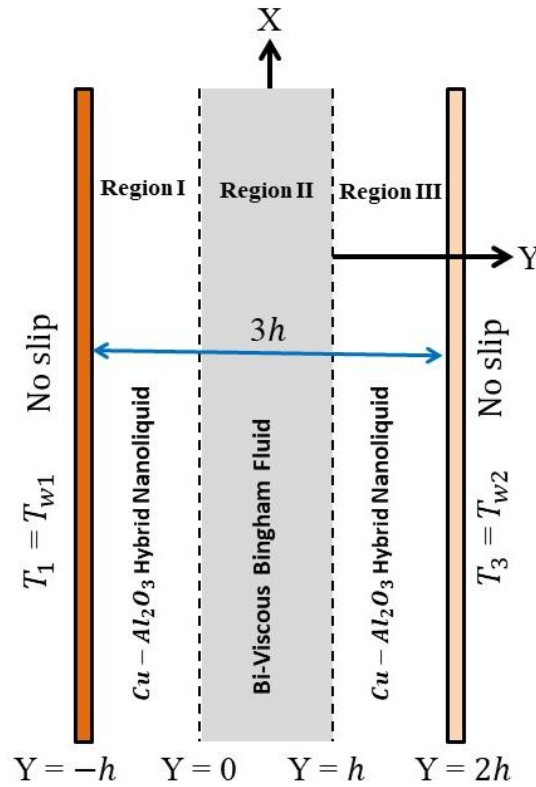\tag{5}
$$

B. Description of the Problem

FIG. 1. Physical configuration.

Fig. 1 illustrates the physical model, which consists of two vertical flat slabs extending upwards in X-direction, and Y-axis is taken normal to the X-axis. The width between the plates is $3h$ and is much smaller than the length of the slabs. Two incompressible immiscible fluids are considered in a three-layer vertical slab. The regions $-h \leq Y \leq 0$ and $h \leq Y \leq 2h$ consists of oil-based $Cu - Al_2O_3$ hybrid nanoliquid having a dynamic viscosity (μ_{hno}), density (ρ_{hno}), thermal expansion coefficients (β_{hno} & β_o^*), and thermal conductivity (k_{hno}). The middle region $0 \leq Y \leq h$ is filled with BVBF having dynamic viscosity (μ_B), density (ρ_B), thermal expansion coefficients (β_B & β_B^*), and thermal conductivity (k_B). The slab walls are kept at distinct constant temperatures i.e., T_{w1} and T_{w2} where $T_{w1} > T_{w2}$. Both walls are impermeable and isothermal. At the two interfaces ($Y = 0$ and $Y = h$), there is a continuity of velocity, shear stress, temperature, and heat flux. The flow of fluids is instigated by a common pressure gradient and nonlinear buoyancy force. It is worth noting that the BVBF and oil-based hybrid nanofluids are immiscible. For instance, pigment-oil-suspensions of printing-ink, polymeric gels, heavy oils, and biopolymers are good examples of BVBF, and it is well known that they cannot be mixed with the base fluid oil. One can choose any two different immiscible fluids.

C. Governing Equations

The general governing equations of mass, momentum, and energy are[4, 22, 38]:

Region I

$$\frac{\partial \rho_{hno}}{\partial t} + \nabla \cdot (\rho_{hno} \boldsymbol{U_1}) = 0 \,, \tag{6}$$

$$\rho_{hno} \left[\frac{\partial \boldsymbol{U_1}}{\partial t} + (\boldsymbol{U_1} \cdot \nabla)\boldsymbol{U_1}\right] = \mu_{hno}\nabla^2\boldsymbol{U_1} - \nabla p + \rho_{hno}\boldsymbol{g} \,, \tag{7}$$

$$(\rho C_p)_{hno} \left[\frac{\partial T_1}{\partial t} + (\boldsymbol{U_1} \cdot \nabla)T_1\right] = -\nabla \cdot (\boldsymbol{q_1} + \boldsymbol{q_{r1}}) + \boldsymbol{\Phi_1} \,, \tag{8}$$

Region II

$$\frac{\partial \rho_B}{\partial t} + \nabla \cdot (\rho_B \boldsymbol{U_2}) = 0 \,, \tag{9}$$

$$\rho_B \left[\frac{\partial \boldsymbol{U_2}}{\partial t} + (\boldsymbol{U_2} \cdot \nabla)\boldsymbol{U_2}\right] = \mu_B \left(1 + \frac{1}{\gamma}\right)\nabla^2\boldsymbol{U_2} - \nabla p + \rho_B\boldsymbol{g} \,, \tag{10}$$

$$(\rho C_p)_B \left[\frac{\partial T_2}{\partial t} + (\boldsymbol{U_2} \cdot \nabla)T_2\right] = -\nabla \cdot (\boldsymbol{q_2} + \boldsymbol{q_{r2}}) + \boldsymbol{\Phi_2} \,, \tag{11}$$

Region III

$$\frac{\partial \rho_{hno}}{\partial t} + \nabla \cdot (\rho_{hno} \boldsymbol{U_3}) = 0 \,, \tag{12}$$

$$\rho_{hno} \left[\frac{\partial \boldsymbol{U_3}}{\partial t} + (\boldsymbol{U_3} \cdot \nabla)\boldsymbol{U_3}\right] = \mu_{hno}\nabla^2\boldsymbol{U_3} - \nabla p + \rho_{hno}\boldsymbol{g} \,, \tag{13}$$

$$(\rho C_p)_{hno} \left[\frac{\partial T_3}{\partial t} + (\boldsymbol{U_3} \cdot \nabla)T_3\right] = -\nabla \cdot (\boldsymbol{q_3} + \boldsymbol{q_{r3}}) + \boldsymbol{\Phi_3} \,. \tag{14}$$

In the above equations, p is the pressure, t is the time, ρ_B and ρ_{hno} are the densities of BVBF and hybrid nanoliquids, μ_B and μ_{hno} are dynamic viscosity of BVBF and hybrid nanoliquids, $(\rho C_p)_B$ and $(\rho C_p)_{hno}$ are the specific heat of BVBF and hybrid nanoliquids, $\boldsymbol{g} = -g\hat{k}$ is the acceleration due to gravity, $\boldsymbol{U_i}$ and T_i $(i = 1, 2, 3)$ are the velocity and temperature of regions I, II, and III respectively, $\boldsymbol{\Phi_i}$, $\boldsymbol{q_i}$ and $\boldsymbol{q_{ri}}$ $(i = 1, 2, 3)$ are viscous dissipation, conduction heat flux, and radiative heat flux of regions I, II, and III respectively, and $\nabla = \frac{\partial}{\partial X}\hat{\imath} + \frac{\partial}{\partial Y}\hat{\jmath} + \frac{\partial}{\partial Z}\hat{k}$ and $\nabla^2 = \frac{\partial^2}{\partial X^2} + \frac{\partial^2}{\partial Y^2} + \frac{\partial^2}{\partial Z^2}$ are gradient and Laplace operators in Cartesian coordinates. The heat fluxes are given by:

$$\boldsymbol{q_1} = -k_{hnf}\nabla T_1 \,, \boldsymbol{q_2} = -k_B\nabla T_2 \,, \text{ and } \boldsymbol{q_3} = -k_{hnf}\nabla T_3,$$

here k_B and k_{hno} are thermal conductivity of BVBF and hybrid nanoliquids.

7

The following assumptions are made in the analysis:

- Flow is fully developed, steady-state, unidirectional, and laminar.
- Since the vertical slabs are infinite in the upward X-direction, the flow variables, viz., velocities and temperatures depend on the Y-coordinate only.
- Fluids obey the quadratic form of the Oberbeck-Boussinesq approximation, that is, the density of fluids is independent of temperature except in the buoyancy terms, and the nonlinear density-temperature relation is accounted for[28, 35].
- The thermophysical effective properties of hybrid nanoliquid depend only on the volume fraction of nanoparticles.
- The fluid properties of oil and BVBF are constant.

Using the assumptions stated above, in (6)-(14), the following equations are obtained[4, 22, 35, 38:]

Region I

$$\frac{dU_1}{dX} = 0 \, , \tag{15}$$

$$\mu_{hno} \frac{d^2 U_1}{dY^2} - \frac{\partial p}{\partial X} + g(\rho\beta)_{hno}(T_1 - T_{w2}) + g\rho_{hno}\beta_o^*(T_1 - T_{w2})^2 = 0 \, , \tag{16}$$

$$k_{hno} \frac{d^2 T_1}{dY^2} - \frac{\partial q_{r1}}{\partial Y} + \mu_{hno} \left(\frac{dU_1}{dY}\right)^2 = 0 \, , \tag{17}$$

Region II

$$\frac{dU_2}{dX} = 0, \tag{18}$$

$$\mu_B \left(1 + \frac{1}{\gamma}\right) \frac{d^2 U_2}{dY^2} - \frac{\partial p}{\partial X} + g(\rho\beta)_B(T_2 - T_{w2}) + g(\rho\beta^*)_B(T_2 - T_{w2})^2 = 0 \, , \tag{19}$$

$$k_B \frac{d^2 T_2}{dY^2} - \frac{\partial q_{r2}}{\partial Y} + \mu_B \left(1 + \frac{1}{\gamma}\right)\left(\frac{dU_2}{dY}\right)^2 = 0 \, , \tag{20}$$

Region III

$$\frac{dU_3}{dX} = 0, \tag{21}$$

$$\mu_{hno} \frac{d^2 U_3}{dY^2} - \frac{\partial p}{\partial X} + g(\rho\beta)_{hno}(T_3 - T_{w2}) + g\rho_{hno}\beta_o^*(T_3 - T_{w2})^2 = 0 \, , \tag{22}$$

$$k_{hno} \frac{d^2 T_3}{dY^2} - \frac{\partial q_{r3}}{\partial Y} + \mu_{hno} \left(\frac{dU_3}{dY}\right)^2 = 0 \, . \tag{23}$$

Furthermore, Eq. (5) becomes

8

$$q_{ri} = -\frac{4\sigma_{SB}}{3a_R}\frac{\partial T_i^4}{\partial Y} \ , \tag{24}$$

To linearize Eq. (24) we use[35]

$$T_i^4 \approx T_{w2}^4 + 4T_{w2}^3 T_i - 4T_{w2}^3 T_{w2}. \tag{25}$$

Because of (25), Eq. (24) yields,

$$q_{ri} = -\frac{16\sigma_{SB}T_{w2}^3}{3a_R}\frac{\partial T_i}{\partial Y} \ . \tag{26}$$

Differentiating (26) with respect to Y gives

$$\frac{\partial q_{ri}}{\partial Y} = -\frac{16\sigma_{SB}T_{w2}^3}{3a_R}\frac{\partial^2 T_i}{\partial Y^2} \ . \tag{27}$$

The first term of Eqs. (16) and (22) represent the viscous term of the hybrid nanoliquid and the first term of Eq. (19) is the viscous term of BVBF. The second term is the common pressure gradient in all regions. The fourth term is due to the quadratic Boussinesq approximation in all regions. In Eqs. (17), (20), and (23), three terms correspond to heat conduction, heat radiation, and viscous dissipation in all regions. The subscripts 1, 2, and 3 represent regions I, II, and III respectively. Subscripts B, o, and hno signify BVBF, oil, and hybrid nanoliquid respectively.

The main feature of the multilayer flow in a vertical slab is the mechanical coupling across the interfaces through the momentum and heat transfer across them. Momentum transfer occurs due to the continuity of the interface tangential velocity and equal shear stress across the interfaces. As far as the thermal coupling is concerned, at the interfaces, the continuity of the temperature, and the balance of the heat flux across the interfaces play an important role. These interface conditions include the conditions of 'no velocity slip' and 'no thermal jump' at the interfaces.

At the left wall of the vertical channel, the zero-velocity and constant temperature are due to the no-slip and isothermal conditions:

$$U_1 = 0 \ , \ \ T_1 = T_{w1} \ \ \text{at} \ \ Y = -h \tag{28a}$$

At the fluid interfaces, the velocity, shear stress, temperature, and heat flux are continuous:

$$U_1 = U_2 \ , \ \ T_1 = T_2 \ , \ \ \mu_{hno}\frac{dU_1}{dY} = \mu_B\left(1 + \frac{1}{\gamma}\right)\frac{dU_2}{dY} \ , \ \ k_{hno}\frac{dT_1}{dY} = k_B\frac{dT_2}{dY} \ , \ \ \text{at} \ \ Y = 0 \tag{28b}$$

$$U_2 = U_3, \quad T_2 = T_3, \quad \mu_B \left(1 + \frac{1}{\gamma}\right)\frac{dU_2}{dY} = \mu_{hno}\frac{dU_3}{dY}, \quad k_B \frac{dT_2}{dY} = k_{hno}\frac{dT_3}{dY}, \quad \text{at } Y = h \qquad (28c)$$

At the right wall of the vertical channel, the zero-velocity and constant temperature are due to the no-slip and isothermal conditions:

$$U_3 = 0, \quad T_3 = T_{w2} \quad \text{at } Y = 2h. \qquad (28d)$$

Eqs. (28a) and (28d) represent the Dirichlet (or first-kind) boundary conditions of velocity and temperature at the left and right walls respectively. These conditions are justified as the velocity and temperature at the liquid-solid boundaries are equal to those at the solid boundary. Eqs. (28b) and (28c) give the boundary conditions at the interfaces i.e., at $Y = 0$ and $Y = h$. These boundary conditions represent continuousness of velocity, shear stress, heat flux, and temperature. The boundary conditions of the interfaces are justified because the last fluid molecule of layer-I got stuck to the first fluid molecule of layer II. Similarly, the last fluid molecule of layer II is glued to the first fluid molecule of layer III.

Having described the mathematical equations, the next subsection focuses on presenting the thermophysical properties used for hybrid nanoliquids.

D. Hybrid Nanoliquid Model

The hybrid nanoliquid considered is made up of oil as a base fluid and a maximum of 4 % of the total volume fraction of nanoparticles (1% of Cu +3% of Al_2O_3). Alumina nanoparticle exhibits important features such as chemical inertness and high stability, but has relatively low thermal conductivity compared to a metallic nanoparticle such as copper (Cu). Through metallic nanoparticles have higher thermal conductivity, their stability and reactivity always hinder their use in nanofluid applications. Combination of a small amount of Cu nanoparticles and Al_2O_3 nanoparticles lead to significant thermo-physical properties along with the stable suspension.

The effective dynamic viscosity and effective thermal conductivity of hybrid nanoliquid are described through modified Brinkman and modified Maxwell models, whereas other properties such as density, and thermal expansion coefficient are described by using the mixture theory. They are given below[19]:

$$\frac{\mu_{hno}}{\mu_o} = \frac{1}{(1-\varphi)^{2.5}}, \qquad (29)$$

$$\frac{k_{hno}}{k_o} = \frac{\left(\frac{\varphi_{Cu}k_{Cu}+\varphi_{Al_2O_3}k_{Al_2O_3}}{\varphi}\right)+2k_o+2\left(\varphi_{Cu}k_{Cu}+\varphi_{Al_2O_3}k_{Al_2O_3}\right)-2\varphi k_o}{\left(\frac{\varphi_{Cu}k_{Cu}+\varphi_{Al_2O_3}k_{Al_2O_3}}{\varphi}\right)+2k_o-\left(\varphi_{Cu}k_{Cu}+\varphi_{Al_2O_3}k_{Al_2O_3}\right)+\varphi k_o} \;, \tag{30}$$

$$\frac{\rho_{hno}}{\rho_o} = (1-\varphi) + \varphi_{Cu}\frac{\rho_{Cu}}{\rho_o} + \varphi_{Al_2O_3}\frac{\rho_{Al_2O_3}}{\rho_o} \;, \tag{31}$$

$$\frac{(\rho\beta)_{hno}}{(\rho\beta)_o} = (1-\varphi) + \varphi_{Cu}\frac{(\rho\beta)_{Cu}}{(\rho\beta)_o} + \varphi_{Al_2O_3}\frac{(\rho\beta)_{Al_2O_3}}{(\rho\beta)_o} \;, \tag{32}$$

where $\varphi(= \varphi_{Cu} + \varphi_{Al_2O_3})$ represents the total nanoparticle volume fraction (NVF) and subscripts Cu and Al_2O_3 represents copper and aluminum oxide nanoparticles. These models are (Eqs. (30)-(32)) valid for the small volume fraction of nanoparticles and particularly Eq. (30) is valid for spherical-shaped nanoparticles. Hence, we have chosen 4% of the total volume fraction and spherical-shaped Cu and Al_2O_3 nanoparticles.

E. Non-dimensionalization

To analyze the problem further and to determine the characteristic quantities, the following dimensionless variables are considered:

$$y = \frac{Y}{h}, \quad u_i = \frac{U_i}{\bar{u}}, \quad \theta_i = \frac{T_i - T_{w2}}{T_{w1} - T_{w2}}, \quad (i = 1, 2, 3) \tag{33}$$

where h is the length scale, $\bar{u}$ is the reference velocity scale, and u_i and θ_i $(i = 1, 2, 3)$ are the dimensionless velocity and temperature of regions I, II, and III respectively. Substituting Eq. (33) into Eqs. (15)-(23) and (28) and using Eqs. (27)-(32), the following dimensionless equations are obtained:

Region I

$$A\frac{d^2u_1}{dy^2} + \lambda\theta_1(B + CQc\theta_1) + P = 0 \;, \tag{34}$$

$$(D + Rd)\frac{d^2\theta_1}{dy^2} + ABr_o\left(\frac{du_1}{dy}\right)^2 = 0 \;, \tag{35}$$

Region II

$$\left(1 + \frac{1}{\gamma}\right)\frac{d^2u_2}{dy^2} + f_v f_r \lambda\theta_2(f_b + f_d Qc\theta_2) + f_v P = 0 \;, \tag{36}$$

$$(1 + f_k Rd)\frac{d^2\theta_2}{dy^2} + Br_B\left(\frac{du_2}{dy}\right)^2 = 0 \;, \tag{37}$$

Region III

$$A\frac{d^2u_3}{dy^2} + \lambda\theta_3(B + CQc\theta_3) + P = 0 \,, \tag{38}$$

$$(D + Rd)\frac{d^2\theta_3}{dy^2} + ABr_o\left(\frac{du_3}{dy}\right)^2 = 0 \,. \tag{39}$$

with boundary conditions

$$\left.\begin{array}{c} u_1 = 0\,, \ \ \theta_1 = 1 \ \ \text{at} \ \ y = -1 \\ u_1 = u_2\,, \ \ \theta_1 = \theta_2\,, \ \ Af_v\frac{du_1}{dy} = \left(1 + \frac{1}{\gamma}\right)\frac{du_2}{dy}\,, \ \ Df_k\frac{d\theta_1}{dy} = \frac{d\theta_2}{dy}\,, \ \ \text{at} \ \ y = 0 \\ u_2 = u_3\,, \ \ \theta_2 = \theta_3\,, \ \ \left(1 + \frac{1}{\gamma}\right)\frac{du_2}{dy} = Af_v\frac{du_3}{dy}\,, \ \ \frac{d\theta_2}{dy} = Df_k\frac{d\theta_3}{dy}\,, \ \ \text{at} \ \ y = 1 \\ u_3 = 0\,, \ \ \theta_3 = 0 \ \ \text{at} \ \ y = 2 \end{array}\right\} \tag{40}$$

where $f_v = \frac{\mu_o}{\mu_B}$, $f_r = \frac{\rho_B}{\rho_o}$, $f_b = \frac{\beta_B}{\beta_o}$, $f_d = \frac{\beta_B^*}{\beta_o^*}$, and $f_k = \frac{k_o}{k_B}$ are ratios of dynamic viscosity, density, first-order thermal expansion coefficient, second-order thermal expansion coefficient, and thermal conductivity respectively, $A = \frac{\mu_{hno}}{\mu_o}$, $B = \frac{(\rho\beta)_{hno}}{(\rho\beta)_o}$, $C = \frac{\rho_{hno}}{\rho_o}$, and $D = \frac{k_{hno}}{k_o}$.

The non-dimensional physical parameters involved in (34)-(40) are

$\lambda = \frac{g\beta_o\rho_o h^2(T_{w1}-T_{w2})}{\mu_o\bar{u}}$ (mixed convection parameter),

$Qc = \frac{\beta_o^*}{\beta_o}(T_{w1} - T_{w2})$, (quadratic convection parameter),

$Rd = \frac{16\sigma_{SB}T_{w2}^3}{3a_R k_o}$, (thermal radiation parameter),

$Br_o = \frac{\mu_o\bar{u}^2}{k_o(T_{w1}-T_{w2})}$, (Brinkman number for oil),

$Br_B = \frac{\mu_B\left(1+\frac{1}{\gamma}\right)\bar{u}^2}{k_B(T_{w1}-T_{w2})}$, (Brinkman number for BVBF), and

$P = -\left(\frac{h^2}{\mu_o\bar{u}}\right)\frac{\partial p}{\partial X}$, (constant pressure gradient parameter).

Eqs. (34)-(39) and boundary conditions (40) constitute a multi-point ordinary differential boundary value problem with six unknowns.

F. Engineering Quantities of Interest

The rate of heat transfer (Nu_l & Nu_r) and skin friction factor (Cf_l & Cf_r) at the walls of the vertical slab are given by

$$Nu_l = \frac{h\left(-k_{hno}\frac{dT_1}{dY}+q_{r1}\right)}{k_o(T_{w1}-T_{w2})}\Bigg|_{Y=-h} \quad \text{(Nusselt number at the left wall)}, \tag{41a}$$

$$Nu_r = \frac{h\left(-k_{hno}\frac{dT_3}{dY}+q_{r3}\right)}{k_o(T_{w2}-T_{w1})}\Bigg|_{Y=2h} \quad \text{(Nusselt number at the right wall)}, \tag{41b}$$

$$Cf_l = \frac{\mu_{hno}\frac{dU_1}{dY}}{\rho_o\bar{u}^2}\Bigg|_{Y=-h} \quad \text{(skin-friction factor at the left wall)}, \tag{42a}$$

$$Cf_r = \frac{\mu_{hno}\frac{dU_3}{dY}}{\rho_o\bar{u}^2}\Bigg|_{Y=2h} \quad \text{(skin-friction factor at the right wall)}. \tag{42b}$$

Because of Eq. (33), we get

$$Nu_l = -[D + Rd]\frac{d\theta_1}{dy}\Bigg|_{y=-1}, \tag{43a}$$

$$Nu_r = [D + Rd]\frac{d\theta_3}{dy}\Bigg|_{y=2}, \tag{43b}$$

$$ReCf_l = A\frac{du_1}{dy}\Bigg|_{y=-1}, \tag{44a}$$

$$ReCf_r = A\frac{du_3}{dy}\Bigg|_{y=2}. \tag{44b}$$

To determine these physical quantities, the four-point boundary value problem defined in (34)-(40) needs to be solved for u_1, u_3, θ_1 and θ_3. In the following subsection, the derivation of entropy equations and Bejan number are presented.

G. Entropy Generation (EG) Analysis

Entropy is the amount of thermal energy in a system per unit of temperature that is not available for useful work. The loss of energy is a crucial factor in production and industrial processes. Increasing entropy will only reduce the efficiency of the system. Therefore, the decisive goal must be to identify the characteristics (parameters) that reduce the generation of entropy by increasing the productivity of the flow system. The second law of thermodynamics

is used to study irreversibility in the form of entropy generation. Viscous dissipation, fluid flow resistance, Joule heating, convective heat transfer, molecular vibrations, thermal radiation, chemical reaction, and heat transfer through finite temperature gradients are some of the parameters that contribute to irreversibility. Following Bejan's work[36, 37,], much research[38-42] has been done on the minimization of entropy production. The local entropy generation rates for regions I, II, and III are as follows:

$$Eg_1 = \frac{1}{T_{w2}^2}\left(k_{hno} + \frac{16\sigma_{SB}T_{w2}^3}{3a_R}\right)\left(\frac{dT_1}{dY}\right)^2 + \frac{\mu_{hno}}{T_{w2}}\left(\frac{dU_1}{dY}\right)^2 , \tag{45}$$

$$Eg_2 = \frac{1}{T_{w2}^2}\left(k_B + \frac{16\sigma_{SB}T_{w2}^3}{3a_R}\right)\left(\frac{dT_2}{dY}\right)^2 + \frac{\mu_B}{T_{w2}}\left(1 + \frac{1}{\gamma}\right)\left(\frac{dU_2}{dY}\right)^2 , \tag{46}$$

$$Eg_3 = \frac{1}{T_{w2}^2}\left(k_{hno} + \frac{16\sigma_{SB}T_{w2}^3}{3a_R}\right)\left(\frac{dT_3}{dY}\right)^2 + \frac{\mu_{hno}}{T_{w2}}\left(\frac{dU_3}{dY}\right)^2 . \tag{47}$$

In Eqs. (45)-(47), the first and second terms on the right side are due to heat conduction, radiative heat transfer, and viscous dissipation. The characteristic entropy generation rate is given by

$$Eg_0 = \frac{k_o(T_{w1}-T_{w2})^2}{h^2 T_{w2}^2} . \tag{48}$$

The characteristic EG rate (given in Eq. (48)) is utilized to obtain the dimensionless local EG number:

$$Ns_1 = (D + Rd)\left(\frac{d\theta_1}{dy}\right)^2 + \left(\frac{ABr_o}{\omega}\right)\left(\frac{du_1}{dy}\right)^2 = HTI_1 + FFI_1, \tag{49}$$

$$Ns_2 = \left(\frac{1}{f_k} + Rd\right)\left(\frac{d\theta_2}{dy}\right)^2 + \left(\frac{Br_B}{\omega f_v}\right)\left(\frac{du_2}{dy}\right)^2 = HTI_2 + FFI_2, \tag{50}$$

$$Ns_3 = (D + Rd)\left(\frac{d\theta_3}{dy}\right)^2 + \left(\frac{ABr_o}{\omega}\right)\left(\frac{du_3}{dy}\right)^2 = HTI_3 + FFI_3. \tag{51}$$

The overall EG through the vertical slab becomes:

$$Ns = Ns_1 + Ns_2 + Ns_3,$$

$$Ns = (D + Rd)\left(\frac{d\theta_1}{dy}\right)^2 + \left(\frac{1}{f_k} + Rd\right)\left(\frac{d\theta_2}{dy}\right)^2 + (D + Rd)\left(\frac{d\theta_3}{dy}\right)^2 + \left(\frac{ABr_o}{\omega}\right)\left(\frac{du_1}{dy}\right)^2 +$$

$$\left(\frac{Br_B}{\omega f_v}\right)\left(\frac{du_2}{dy}\right)^2 + \left(\frac{ABr_o}{\omega}\right)\left(\frac{du_3}{dy}\right)^2 , \tag{52}$$

where $HTI_{1,3} = (D + Rd)\left(\frac{d\theta_{1,3}}{dy}\right)^2$, $HTI_2 = \left(\frac{1}{f_k} + Rd\right)\left(\frac{d\theta_2}{dy}\right)^2$, $FFI_{1,3} = \left(\frac{ABr_o}{\omega}\right)\left(\frac{du_{1,3}}{dy}\right)^2$,

$FFI_2 = \left(\frac{Br_B}{\omega f_v}\right)\left(\frac{du_2}{dy}\right)^2$ and $\omega = \frac{T_{w1} - T_{w2}}{T_{w2}}$ is characteristic temperature ratio.

In (52), the first three terms represent heat transfer irreversibility (HTI) due to heat conduction and radiation, and the last three terms represent fluid friction irreversibility (FFI).

The dominant irreversibility mechanism is practically significant as total entropy is inadequate to overcome this problem. The Bejan number is useful to understand the relative effects of fluid friction and heat transfer. The Bejan number is the ratio of the thermal entropy to the total entropy. The Bejan number for the multi-layer problem is given by

$$Be = \frac{\sum_{i=1}^{3} HTI_i}{\sum_{i=1}^{3} HTI_i + \sum_{i=1}^{3} FFI_i} = \frac{\sum_{i=1}^{3} HTI_i}{Ns}. \tag{53}$$

The Bejan number (Be) has values that vary between 0 and 1. The inferences obtained for the Bejan number can be categorized into three cases.

- $Be < 0.5$ indicates that the EG is mainly due to the viscous dissipation i.e., the FFI dominates over HTI.
- $Be > 0.5$ indicates that the EG is mainly due to the heat transfer (convective-radiative) i.e., HTI dominates over the FFI.
- $Be = 0.5$ indicates that FFI and HTI are of the same order.

Having Bejan number and entropy equations derived, we shall now move on to solving the four-point boundary value problem defined in (34)-(40).

III. METHOD OF SOLUTION AND VALIDATION

Eqs. (34)-(40) represents the nonlinear multi-point (four-point) boundary value problem and is solved by DTM.

A. DTM Procedure

DTM is a semi-analytical approach that uses the Taylor series expansion to find analytical solutions, which was introduced by Zhou[43]. To acquire the differential transform of the dimensionless governing equations and boundary conditions, certain transformation rules are applied. The benefit of using the transformation method is that it makes a seemingly difficult problem simple and nonlinear differential equations can be directly handled without any

linearization, perturbation, or discretization. Applications of DTM to the fluid flow problems can be found in[44-46]. The definition of one-dimensional DTM is:

$$\mathcal{F}_l(b) = \frac{1}{b!}\left[\frac{d^b f_l(y)}{dy^b}\right]_{y=y_0} , \tag{54}$$

and the inverse differential transformation is given by

$$f_l(y) = \sum_{b=0}^{\infty} \mathcal{F}_l(b)(y - y_0)^b . \tag{55}$$

For execution purposes, $f_l(y)$ can be written as a finite series and hence Eq. (55) can be written as

$$f_l(y) = \sum_{b=0}^{n} \mathcal{F}_l(b)(y - y_0)^b , \tag{56}$$

where n is taken depending on the convergence criteria and $\mathcal{F}_l(b)$ is the differential transform of $f_l(y)$. From the definitions of (54) and (55), certain fundamental theorems of the one-dimensional differential transform are as follows:

Theorem 1: If $f(y) = w(y) \pm z(y)$ then $\mathcal{F}(b) = \mathcal{W}(b) \pm \mathcal{Z}(b)$, where $\mathcal{W}(b)$ and $\mathcal{Z}(b)$ are differential transforms of $w(y)$ and $z(y)$ respectively.

Theorem 2: If $f(y) = \kappa w(y)$ then $\mathcal{F}(b) = \kappa \mathcal{W}(b)$, where κ is a constant.

Theorem 3: If $f(y) = \frac{d^m w(y)}{dy^m}$ then $\mathcal{F}(b) = \frac{(b+m)!}{b!}\mathcal{W}(b + m)$.

Theorem 4: If $f(y) = w(y)z(y)$ then $\mathcal{F}(b) = \sum_{a=0}^{b} \mathcal{W}(a)\mathcal{Z}(b - a)$.

Theorem 5: If $f(y) = y^m$ then $\mathcal{F}(b) = \delta(b - m)$, where $\delta(b - m) = \begin{cases} 1 & \text{if } b = m \\ 0 & \text{if } b \neq m \end{cases}$.

TABLE I. One-dimensional differential transform of certain functions.

Original function	Transformed function
$\dfrac{d^2 u_i}{dy^2}$	$(b + 1)(b + 2)\mathcal{U}_i[b + 2]$
$\dfrac{d^2 \theta_i}{dy^2}$	$(b + 1)(b + 2)\Theta_i[b + 2]$
y^0	$\delta[b]$
$\theta_i(y)$	$\Theta_i[b]$

16

θ_i^2	$\displaystyle\sum_{a=0}^{b} \Theta_i[a]\Theta_i[b-a]$
$\left(\dfrac{du_i}{dy}\right)^2$	$\displaystyle\sum_{a=0}^{b} (a+1)(b-a+1)\,\mathcal{U}_i[b-a+1]\mathcal{U}_i[a+1]$
where $i = 1, 2, 3$.	

Table I presents the differential transformations of some functions and their derivatives. Using Table I, applying the differential transform to Eqs. (34)-(39), we obtain:

Region I

$$A(b+1)(b+2)\mathcal{U}_1[b+2] + \lambda\left(B\Theta_1[b] + CQc\sum_{a=0}^{b}\Theta_1[a]\Theta_1[b-a]\right) +$$
$$P\delta[b] = 0 , \qquad (57)$$

$$(b+1)(b+2)\Theta_1[b+2](D+Rd) + ABr_o\sum_{a=0}^{b}(a+1)(b-a+1)\,\mathcal{U}_1[b-a+$$
$$1]\mathcal{U}_1[a+1] = 0 , \qquad (58)$$

Region II

$$\left(1+\frac{1}{\gamma}\right)(b+1)(b+2)\mathcal{U}_2[b+2] + f_v f_r \lambda\left(f_b\Theta_2[b] + f_d Qc\sum_{a=0}^{b}\Theta_2[a]\Theta_2[b-a]\right) +$$
$$f_v P\delta[b] = 0, \qquad (59)$$

$$(b+1)(b+2)\Theta_2[b+2](1+f_k Rd) + Br_B\sum_{a=0}^{b}(a+1)(b-a+$$
$$1)\,\mathcal{U}_2[b-a+1]\mathcal{U}_2[a+1] = 0 , \qquad (60)$$

Region III

$$A(b+1)(b+2)\mathcal{U}_3[b+2] + \lambda\left(B\Theta_3[b] + CQc\sum_{a=0}^{b}\Theta_3[a]\Theta_3[b-a]\right) +$$
$$P\delta[b] = 0 , \qquad (61)$$

$$(b+1)(b+2)\Theta_3[b+2](D+Rd) + ABr_o\sum_{a=0}^{b}(a+1)(b-a+1)\,\mathcal{U}_3[b-a+$$
$$1]\mathcal{U}_3[a+1] = 0 , \qquad (62)$$

where $\mathcal{U}_i(b)$ and $\Theta_i(b)$ are the transformed notations of $u_i(y)$ and $\theta_i(y)$ respectively.

To apply the differential transform to the boundary conditions, they must be first transformed to initial conditions. Hence, the boundary conditions (40) are considered as follows:

$$u_1(0) = u_2(0) = 0, \quad \frac{d}{dy}u_2(0) = \alpha_2, \quad u_3(0) = \alpha_3,$$

$$\frac{d}{dy}u_3(0) = \alpha_4, \quad Af_v\frac{d}{dy}u_1(0) = \left(1 + \frac{1}{\gamma}\right)\alpha_2,$$

$$\theta_1(0) = \theta_2(0) = \epsilon_1, \quad \frac{d}{dy}\theta_2(0) = \epsilon_2, \quad \theta_3(0) = \epsilon_3,$$

$$\frac{d}{dy}\theta_3(0) = \epsilon_4, \quad Df_k\frac{d}{dy}\theta_1(0) = \epsilon_2. \tag{63}$$

where α_i and ϵ_i are unknowns to determine. For the initial conditions (Eq. (63)), we apply the differential transformation and get

$$\mathcal{U}_1[0] = \mathcal{U}_2[0] = \alpha_1, \quad \mathcal{U}_2[1] = \alpha_2, \quad \mathcal{U}_3[0] = \alpha_3, \quad \mathcal{U}_3[1] = \alpha_4,$$

$$\mathcal{U}_1[1] = \left(\frac{1}{Af_v}\right)\left(1 + \frac{1}{\gamma}\right)\alpha_2,$$

$$\Theta_1[0] = \Theta_2[0] = \epsilon_1, \quad \Theta_2[1] = \epsilon_2, \quad \Theta_3[0] = \epsilon_3, \quad \Theta_3[1] = \epsilon_4,$$

$$\Theta_1[1] = \left(\frac{1}{Df_k}\right)\epsilon_2. \tag{64}$$

Substituting (64) in (57)-(62) and by recursive method, several values of $\mathcal{U}_i[v]$ and $\Theta_i[v]$ can be calculated. The series solution for the transformed functions of $u_i(y)$ and $\theta_i(y)$ are given as:

$$u_i(y) = \sum_{b=0}^{n} \mathcal{U}_i(b)y^b, \tag{65}$$

$$\theta_i(y) = \sum_{b=0}^{n} \Theta_i(b)y^b. \tag{66}$$

Now substituting all the values of $\mathcal{U}_i[b]$ and $\Theta_i[b]$ into (65) and (66), the series solutions for the regions I, II, and III are obtained respectively. Then, the values for the unknown constants are found using the boundary conditions at $y = -1, 1$ and 2 which can be acquired from Eq. (40). The solutions are obtained for the velocity and temperature of the regions I, II, and III when $P = Rd = \lambda = 2$, $Qc = Br_O = 0.2$, $Br_B = 0.6$, $\gamma = 0.5$, $\varphi_{Cu} = 1\%$ and $\varphi_{Al_2O_3} = 3\%$.

Region I

$$u_1(y) = 2.8319 + 0.7921y - 2.0361y^2 + 0.1108y^3 + 0.1011y^4 - 0.0901y^5 + 0.0097y^6 - 0.0087y^7 - 0.0061y^8 + 0.0039y^9 - 0.0016y^{10} + 0.0025y^{11} + 0.0018y^{12} - 0.0009y^{13} + 0.0012y^{14} - 0.0025y^{15} - 0.0086y^{16} + 0.0009y^{17} - 0.0005y^{18} + 0.0007y^{19} + 0.0043y^{20}. \tag{67}$$

$$\theta_1(y) = 1.0322 - 0.5311y - 0.1896y^2 + 0.4137y^3 - 0.2972y^4 + 0.2792y^5 + 0.2594y^6 - 0.1872y^7 + 0.1804y^8 - 0.1043y^9 - 0.0774y^{10} + 0.0484y^{11} -$$

18

$$0.0109y^{12} - 0.0098y^{13} + 0.0087y^{14} - 0.0074y^{15} + 0.0045y^{16} + 0.0038y^{17} -$$
$$0.0009y^{18} + 0.0005y^{19} - 0.0001y^{20}. \tag{68}$$

Region II

$$u_2(y) = 2.8319 + 1.1829y - 1.4056y^2 + 0.0099y^3 + 0.0055y^4 - 0.0045y^5 +$$
$$0.0024y^6 - 0.0009y^7 - 0.0003y^8 + 0.0001y^9 - 9.9812 * 10^{-4}y^{10} + 7.0214 *$$
$$10^{-4}y^{11} + 1.1438 * 10^{-4}y^{12} - 7.8411 * 10^{-5}y^{13} + 1.1541 * 10^{-5}y^{14} - 1.4333 *$$
$$10^{-5}y^{15} - 8.1054 * 10^{-6}y^{16} + 5.4144 * 10^{-7}y^{17} - 9.1349 * 10^{-8}y^{18} + 3.1144 *$$
$$10^{-9}y^{19} + 1.4545 * 10^{-9}y^{20}. \tag{69}$$

$$\theta_2(y) = 1.0322 - 0.0059y - 0.2693y^2 + 0.2151y^3 - 0.1919y^4 + 0.0937y^5 +$$
$$0.0103y^6 - 0.0092y^7 + 0.0017y^8 - 0.0001y^9 - 9.8317 * 10^{-5}y^{10} + 5.1743 *$$
$$10^{-5}y^{11} - 1.8413 * 10^{-5}y^{12} - 8.7928 * 10^{-6}y^{13} + 7.8218 * 10^{-6}y^{14} - 5.4027 *$$
$$10^{-6}y^{15} + 2.7381 * 10^{-6}y^{16} + 9.7289 * 10^{-7}y^{17} - 5.2639 * 10^{-7}y^{18} + 3.1049 *$$
$$10^{-7}y^{19} - 1.8491 * 10^{-8}y^{20}. \tag{70}$$

Region III

$$u_3(y) = 2.1418 + 3.0759y - 2.8793y^2 + 0.1207y^3 + 0.2418y^4 - 0.1181y^5 +$$
$$0.0279y^6 + 0.0098y^7 - 0.0037y^8 + 0.0017y^9 - 3.2991 * 10^{-5}y^{10} + 9.1432 *$$
$$10^{-9}y^{11} + 3.9421 * 10^{-9}y^{12} - 2.2421 * 10^{-9}y^{13} + 1.4218 * 10^{-9}y^{14} + 1.1421 *$$
$$10^{-9}y^{15} - 9.8467 * 10^{-10}y^{16} + 1.4317 * 10^{-10}y^{17} + 9.1342 * 10^{-11}y^{18} -$$
$$5.4312 * 10^{-11}y^{19} + 1.2147 * 10^{-12}y^{20}. \tag{71}$$

$$\theta_3(y) = 1.1911 - 0.0233y - 0.5101y^2 + 0.3798y^3 - 0.1551y^4 - 0.0083y^5 +$$
$$0.0144y^6 - 0.0085y^7 + 0.0005y^8 + 0.0024y^9 - 4.7512 * 10^{-4}y^{10} + 8.1423 *$$
$$10^{-8}y^{11} - 8.1285 * 10^{-8}y^{12} - 1.3221 * 10^{-9}y^{13} + 6.1210 * 10^{-12}y^{14} - 5.9037 *$$
$$10^{-12}y^{15} + 9.6528 * 10^{-14}y^{16} + 9.0816 * 10^{-14}y^{17} - 7.0214 * 10^{-14}y^{18} +$$
$$1.1258 * 10^{-14}y^{19} - 1.0254 * 10^{-14}y^{20} . \tag{72}$$

In the next subsection, the validation of DTM and convergence analysis is performed.

B. Convergence Analysis and Validation

To affirm accuracy, the results obtained by DTM are compared with those obtained using MATLAB solver (*bvp5c*). *Bvp5c* method[44] is a four-stage Lobatto IIIa formula-based finite

difference algorithm. It produces a continuous solution on the interval $[p, q]$ that has a uniform fifth-order precision. Eqs. (34)-(40) represent the four-point boundary value problem (BVP). Since *bvp5c* only accepts two-point BVPs, Eqs. (34)-(40) needs to be converted to a two-point boundary value problem using the following transformations.

$y = \tau + 1$, (Transformation for region II),

$y = \eta + 2$, (Transformation for region III).

Detailed procedures for handling multipoint BVP can be found in[44]. The comparison results are presented in Table II and imply that the DTM results are accurate to at least 6 decimal places.

The viscous dissipation term makes the energy equation non-linear and couples with the momentum equation, consequently the system of differential equations becomes complex. Therefore, convergence analyzes of DTM solutions are performed in the presence and absence of viscous dissipation. Tables III and IV depict the convergence analysis of the DTM in the presence and absence of viscous dissipation. In the absence of viscous dissipation (Table III), the convergent solutions are attained by considering 4th-order approximation. Table III also present the comparison of DTM solutions and *bvp5c* solutions and exact solutions (in the absence of viscous dissipation, see Appendix A). While in the presence of viscous dissipation (Table IV), even 10th-order approximations are not sufficient since the values are far from precise. As seen in Table IV, the accuracy of the first digit is obtained from the 12th-order approximation. However, from the 20th-order approximation, a precision greater than 6 decimal places is achieved. Therefore, the simulations are performed with an approximation of order 20.

TABLE II. Comparison of velocity and temperature values obtained from DTM and *bvp5c*.

	Velocity		Temperature	
y	DTM	bvp5c	DTM	bvp5c
-1	0	0	1	1
-0.75	1.100618	1.100618	1.080621	1.080621
-0.5	1.940173	1.940173	1.093648	1.093648
-0.25	2.516060	2.516060	1.070361	1.070361
0	2.831866	2.831866	1.032213	1.032213
0.25	3.001208	3.001208	1.011343	1.011343

0.5	3.024162	3.024162	0.985634	0.985634
0.75	2.900745	2.900745	0.957625	0.957625
1	2.630976	2.630976	0.913679	0.913679
1.25	2.252901	2.252901	0.726891	0.726891
1.5	1.668629	1.668629	0.523026	0.523026
1.75	0.907340	0.907340	0.286468	0.286468
2	0	0	0	0

TABLE III. Convergence analysis of DTM without viscous dissipation, and comparison of DTM results with bvp5c results and exact solutions.

y	2nd order approx	4th order approx	bvp5c	2nd order approx	4th order approx	bvp5c	Exact solution
	Velocity			Temperature			
-1	0	0	0	1	1	1	1
-0.75	0.895258	0.931074	0.931074	0.892769	0.892769	0.892769	0.892770
-0.5	1.606694	1.630557	1.630557	0.785538	0.785538	0.785538	0.785539
-0.25	2.134309	2.114975	2.114975	0.678308	0.678308	0.678308	0.678309
0	2.478101	2.400236	2.400236	0.571077	0.571077	0.571077	0.571078
0.25	2.730462	2.573721	2.573721	0.535538	0.535538	0.535538	0.535539
0.5	2.836700	2.601102	2.601102	0.500000	0.500000	0.500000	0.500000
0.75	2.796814	2.482399	2.482399	0.464462	0.464462	0.464462	0.464461
1	2.610805	2.217631	2.217631	0.428923	0.428923	0.428923	0.428922
1.25	2.297236	1.876249	1.876249	0.321692	0.321692	0.321692	0.321691
1.5	1.757579	1.384139	1.384139	0.214462	0.214462	0.214462	0.214461
1.75	0.991834	0.754523	0.754523	0.107231	0.107231	0.107231	0.107230
2	0	0	0	0	0	0	0

TABLE IV. Convergence analysis of DTM with viscous dissipation.

y	4th order approx	10th order approx	12th order approx	14th order approx	16th order approx	20th order approx	bvp5c
	Velocity						
-1	0	0	0	0	0	0	0
-0.75	1.731861	1.303178	1.298597	1.114789	1.100825	1.100618	1.100618

-0.5	3.108892	2.305829	1.974592	1.968745	1.940224	1.940173	1.940173
-0.25	4.074375	2.968084	2.634875	2.587451	2.516174	2.516060	2.516060
0	4.579023	3.257775	2.978215	2.854789	2.831958	2.831866	2.831866
0.25	4.839717	3.305099	3.142135	3.095231	3.001385	3.001208	3.001208
0.5	4.953001	3.205415	3.194713	3.099127	3.024274	3.024162	3.024162
0.75	4.918832	2.958687	2.919781	2.907541	2.900857	2.900745	2.900745
1	4.737144	2.864892	2.705231	2.665743	2.630981	2.630976	2.630976
1.25	4.289903	2.403867	2.375417	2.298674	2.252941	2.252901	2.252901
1.5	3.348455	1.914935	1.798745	1.695321	1.668755	1.668629	1.668629
1.75	1.918822	1.171811	0.999241	0.954712	0.907754	0.907340	0.907340
2	0	0	0	0	0	0	0
Temperature							
-1	1	1	1	1	1	1	1
-0.75	1.516080	1.308960	1.195417	1.098754	1.080847	1.080621	1.080621
-0.5	1.858774	1.522067	1.198473	1.099879	1.093818	1.093648	1.093648
-0.25	2.101797	1.684341	1.187142	1.094571	1.070587	1.070361	1.070361
0	2.303650	1.828746	1.174215	1.091427	1.032477	1.032213	1.032213
0.25	2.352695	1.874710	1.141257	1.035471	1.011572	1.011343	1.011343
0.5	2.387170	1.919056	0.998756	0.990127	0.985874	0.985634	0.985634
0.75	2.419674	1.950716	0.985746	0.967458	0.957847	0.957625	0.957625
1	2.446363	1.942296	0.985298	0.957412	0.913847	0.913679	0.913679
1.25	2.444629	1.804243	0.856874	0.764178	0.726974	0.726891	0.726891
1.5	2.221470	1.595281	0.652418	0.554782	0.523274	0.523026	0.523026
1.75	1.531638	1.152542	0.599658	0.298657	0.286642	0.286468	0.286468
2	0	0	0	0	0	0	0

Having discussed the solution procedure, the next section focuses on the discussion of the results obtained.

IV.   RESULTS AND DISCUSSION

The flow and heat transport in BVBF sandwiched between $Cu - Al_2O_3 - H_2O$ hybrid nanoliquids subjected to nonlinear convection, thermal radiation, and viscous dissipation are investigated. The values for quadratic convection parameter (Qc), Brinkman number for oil

(Br_o), Brinkman number for BVBF (Br_B), mixed convection parameter (λ), radiation parameter (Rd), BVBF parameter (γ), and NVF $(\varphi_{Cu}$ & $\varphi_{Al_2O_3})$ for simulations are taken as $\lambda = 2$, $Qc = 0.2$, $Br_O = 0.2$, $Br_B = 0.6$, $P = 2$, $Rd = 2$, $\gamma = 0.5$, $\varphi_{Cu} = 1\%$ and $\varphi_{Al_2O_3} = 3\%$. The effects of these physical parameters are presented graphically (see Figs. 2-13).

The influence of the quadratic convection parameter (Qc) on the velocity and temperature fields is shown in Fig. 2 (a) & (b). Increasing the values of the quadratic convection parameter leads to an improvement of the velocity and temperature fields in all the regions and thus improves the situation of heat transport in the system. It is worth noting that $Qc = 0$ represents the conventional linear Boussinesq approximation (LBA) model and $Qc \neq 0$ denotes the quadratic (nonlinear) Boussinesq approximation (QBA) model. Due to the consideration of the quadratic density-temperature change in terms of the buoyancy force, the thermal buoyancy force becomes stronger. The increase in thermal buoyancy is accountable for the increasing effect on the distribution of velocity and temperature. Furthermore, the magnitude of velocity and temperature are greater when the quadratic Boussinesq approximation is taken into account than the linear Boussinesq approximation. Due to the predominant impact of nonlinear density-temperature variation on flow distributions, it cannot be ignored as stated before. Furthermore, quadratic convection has a greater impact on the velocity in the center of the slab, while near the walls its impact is minute. Our results of quadratic thermal convection are similar to those reported by Partha[30], and Shaw *et al*[31].
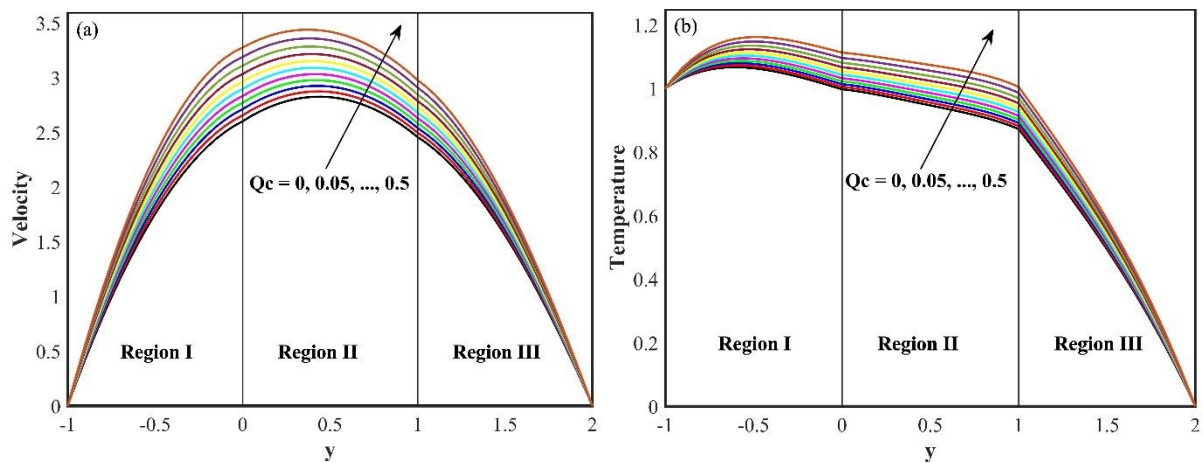
FIG. 2. Influence of Qc on (a) velocity and (b) temperature.

Fig. 3 (a) & (b) demonstrates the consequence of the mixed convection parameter (λ) on the velocity and temperature fields. The velocity and temperature fields depict an increasing trend as the values of the mixed convection parameter increase in all the regions. By definition,

λ is the ratio of Reynolds number to the Grashof number. So, an increase in the mixed convection parameter values induces an increase in the buoyancy force. Since buoyancy forces promote the flow of fluid molecules, a tendency to increase in velocity and temperature fields can be observed. The results for mixed convection are analogous to those reported by Vajravelu et al.[23] and Partha[30].
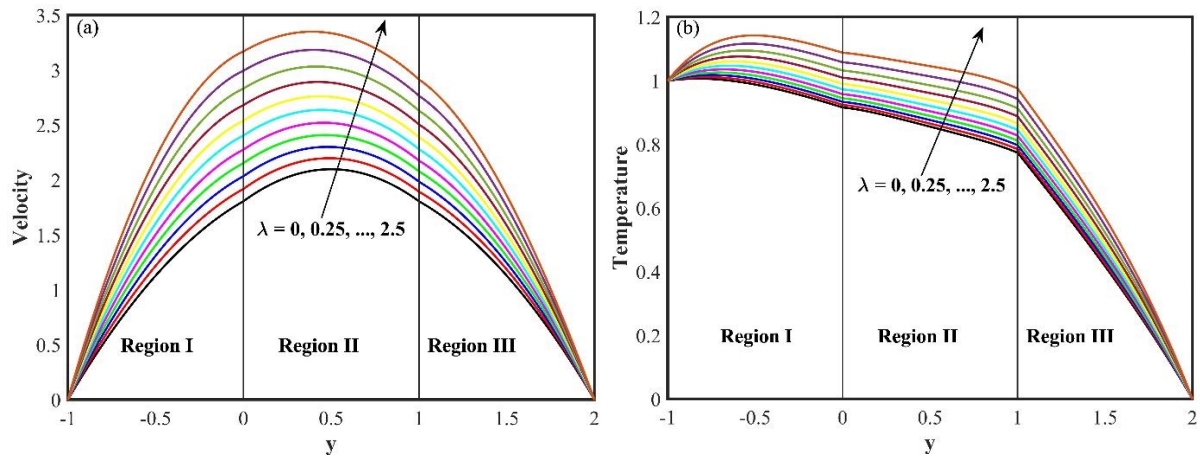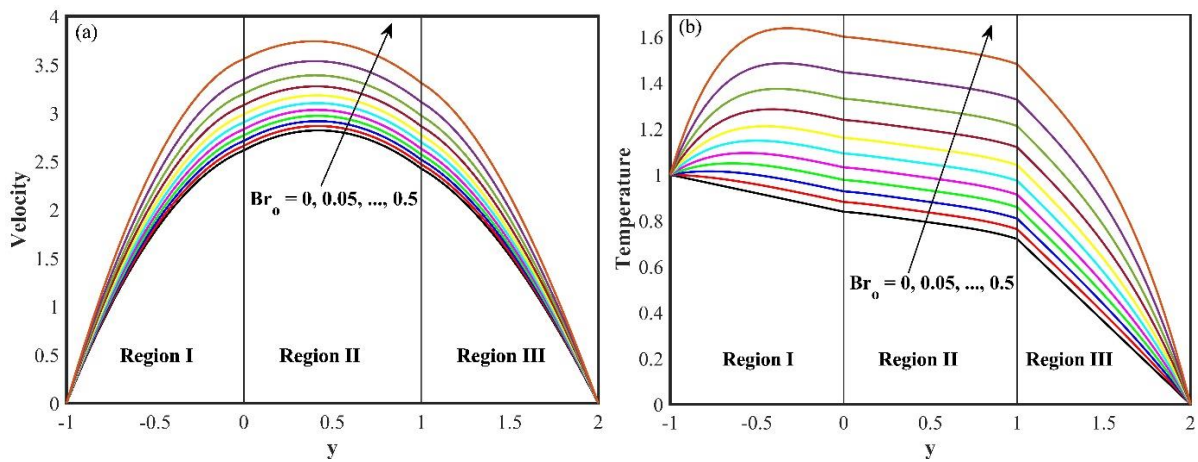

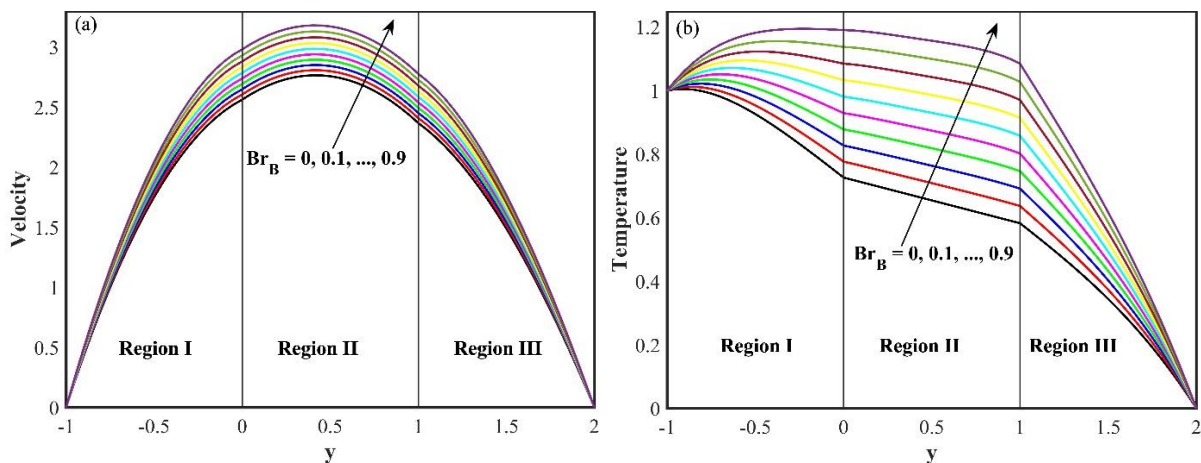**FIG. 3.** Influence of λ on (a) velocity and (b) temperature

Figs. 4 and 5 describe the effect of the Brinkman number for oil (Br_o) and Brinkman number for BVBF (Br_B) respectively on the velocity and temperature fields. The zero value of the Brinkman numbers represents the fluid system without viscous heating. An increase in the Brinkman numbers causes a rise in the velocity and temperature fields, in all regions. The Brinkman number is directly related to kinetic energy. As the Brinkman number rises, the kinetic energy of the fluid system improves as expected. Higher kinetic energy is accountable for a higher fluid temperature, which leads to an improvement in the magnitude of the velocity. The Brinkman number is a crucial parameter in polymer processing. The results for the Brinkman number are similar to those reported by Murthy and Srinivas[38]. The Brinkman number for oil has a predominant effect on the temperature field in region I and III over region II. Likewise, the Brinkman number for BVBF has a predominant influence on the temperature field in region II compared to other regions.

The influence of the radiation parameter (Rd) on the velocity and temperature fields is shown in Fig. 6 (a) & (b). As the radiation parameter decreases, an increasing trend for both velocity and temperature fields is observed, in all the regions. The effect of radiation dampens the effect of natural convection by decreasing the variation of the velocity and temperature fields. The effect of radiation is known to reduce the rate of energy transfer to the liquid. Furthermore, it can be noted that from the definition of the radiation parameter, the radiation
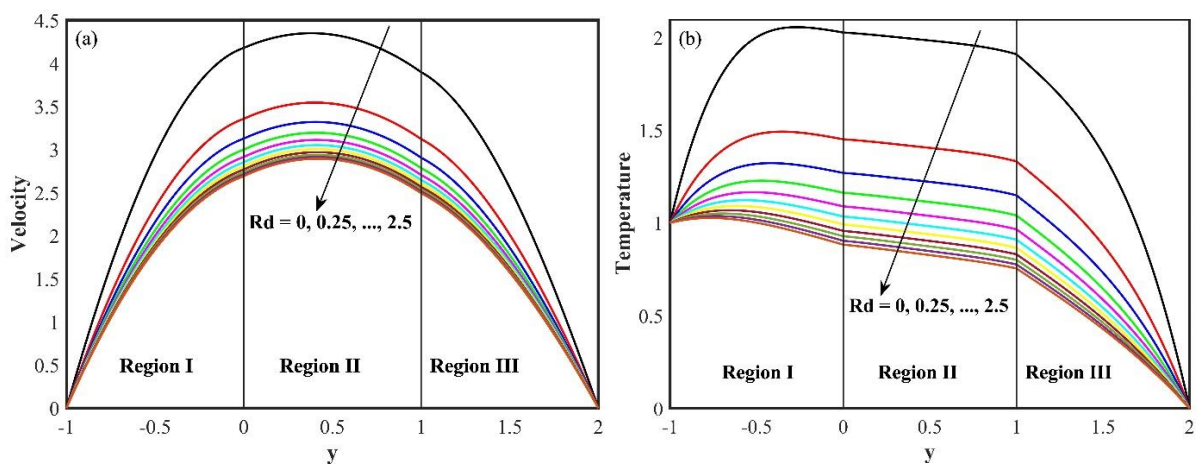
factor is inversely related to heat conduction. Therefore, an increasing trend in temperature is observed for lower values of the radiation factor.

FIG. 4. Influence of Br_o on (a) velocity and (b) temperature

FIG. 5. Influence of Br_B on (a) velocity and (b) temperature

FIG. 6. Influence of Rd on (a) velocity and (b) temperature

Fig. 7 (a) and (b) describe the effect of the BVBF parameter (γ) on the velocity and temperature fields. We deliberately include the BVBF parameter (γ) in the definition of Brinkman number for BVBF (Br_B) so that Br_B has a difference between the Brinkman number for oil (Br_o). Since, Br_B is a function of γ, by varying γ, the value of Br_B also varies. Here to analyze the effects of BVBF parameter (γ), we have chosen $\gamma = [0.05, 0.08, 0.1, 0.2, 0.25,$ $0.4, 0.5, 0.8,\ 1.0,\ 2.0,\ 2.5]$ and the corresponding Br_B values chosen are $[4.2, 2.7, 2.2, 1.2, 1,$ $0.7, 0.6, 0.45, 0.4, 0.3, 0.28]$. Due to this, the velocity and temperature distributions are more pronounced in the BVBF layer (region II) than in other layers (regions I and III). It is found that the effect of increasing the BVBF parameter is to increase the velocity and temperature fields as expected. An increase in the BVBF parameter physically means a decrease in apparent viscosity, which supports the fluid momentum. Therefore, the velocity and temperature fields increase with the BVBF parameter.
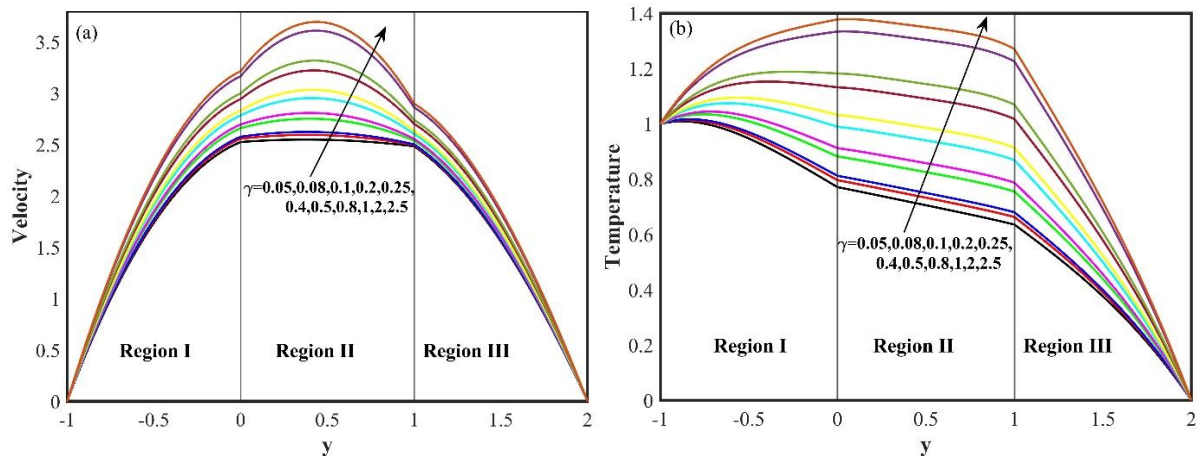

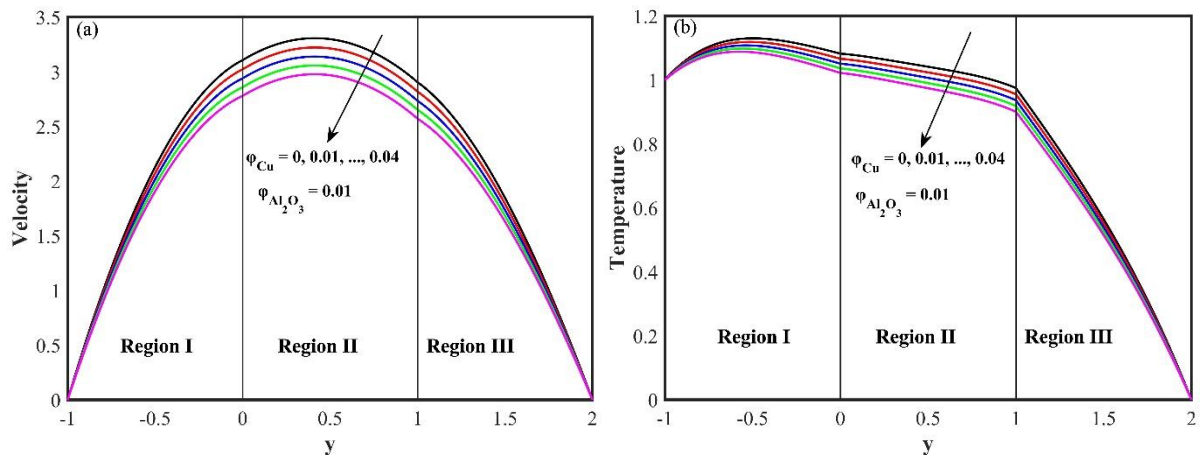**FIG. 7.** Influence of γ on (a) velocity and (b) temperature

FIG. 8. Influence of φ_{Cu} on (a) velocity and (b) temperature

Figs. 8 & 9 show the impact of NVF (φ_{Cu} & $\varphi_{Al_2O_3}$) on the velocity and temperature fields. Both velocity and temperature have a diminishing effect as the values of φ_{Cu} and $\varphi_{Al_2O_3}$ are increased in all the regions. The presence of nanoparticles causes the fluid to be highly denser, and as a result, the momentum of the fluid diminished. Though the inclusion of nanoparticles was restricted to regions I and III, the impact of NVF can be noticed in all the regions, including region II (BVBF layer). This is because of the interfacial condition, which is the equality of temperature and heat fluxes at the interface. The results for NVF are similar to those reported by Rajeev and Mahanthesh[35].
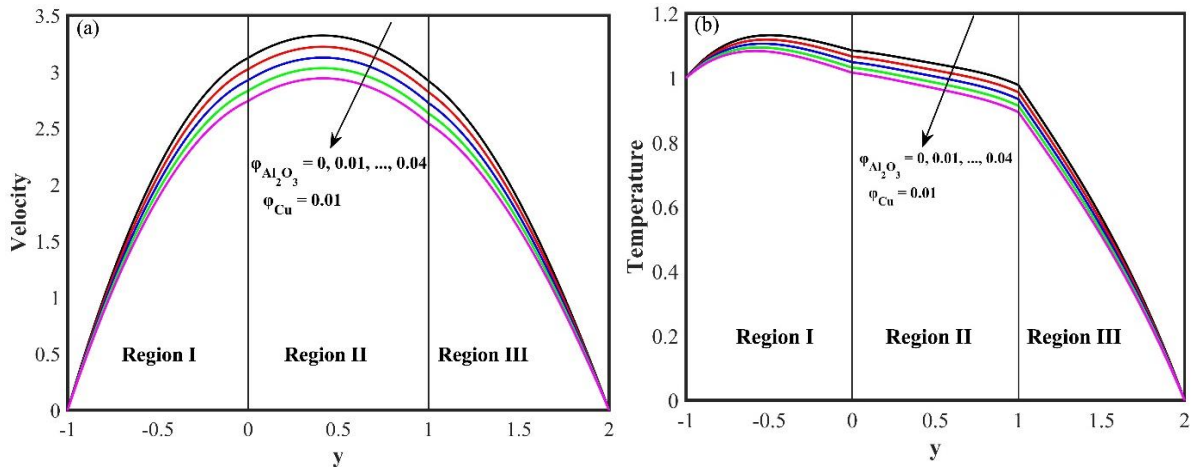

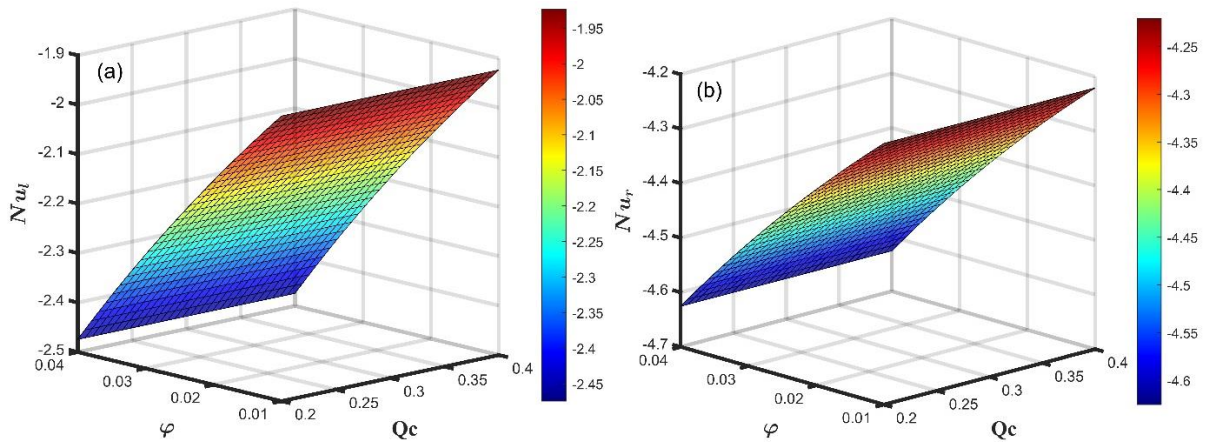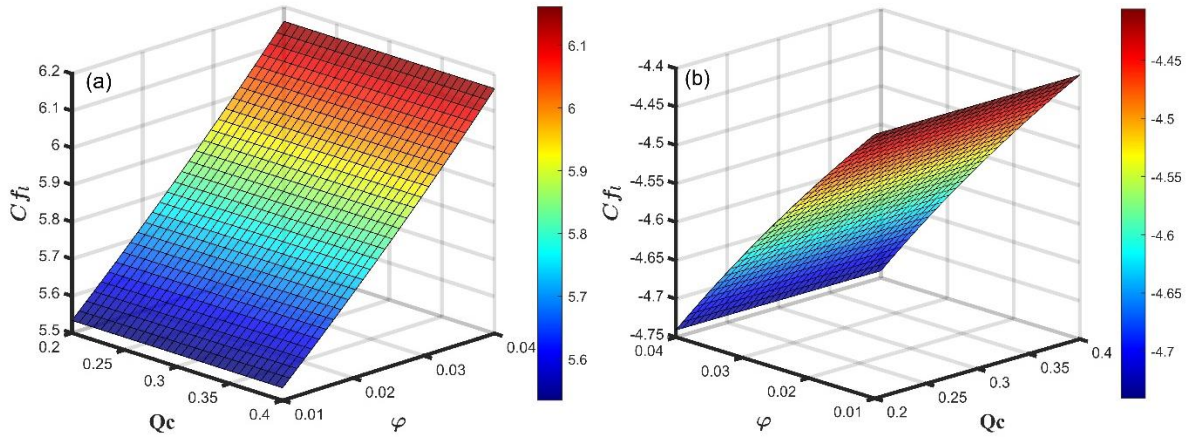**FIG. 9.** Influence of $\varphi_{Al_2O_3}$ on (a) velocity and (b) temperature.

FIG. 10. Influence of total volume fraction (φ) and nonlinear convection (Qc) on (a) Nu_l, and (b) Nu_r.

**FIG. 11.** Influence of total volume fraction (φ) and nonlinear convection (Qc) on (a) Cf_l, and (b) Cf_r.

Figs. 10 and 11 represent the effects of the NVF (φ) and quadratic convection parameter (Qc) on the Nusselt number (Nu_l & Nu_r) and skin friction (Cf_l & Cf_r) of both left and right walls. The Nusselt number of the left and right walls (as in Fig. 10 (a) & (b)) is seen to upsurge as the values of φ increases and reduces as the values of Qc increase. This is because the thickness of the boundary layer on the left wall has condensed due to the increase in the value of φ. As a result, the Nusselt number on the left wall has improved. Whereas a thicker thermal boundary layer on the left wall due to a large Qc leads to a reduced Nusselt number. In Fig. 11 (a), the skin friction coefficient on the left wall improved with Qc and φ. In Fig. 11 (b), the skin friction coefficient on the right wall gets enhanced with φ, while it gets reduced due to higher Qc values. To summarize, Nu_l & Nu_r is maximum for high values of φ and low values of Qc. Cf_l is minimum for low values of φ and Qc. Cf_r is minimum for high values of Qc and low values of φ.
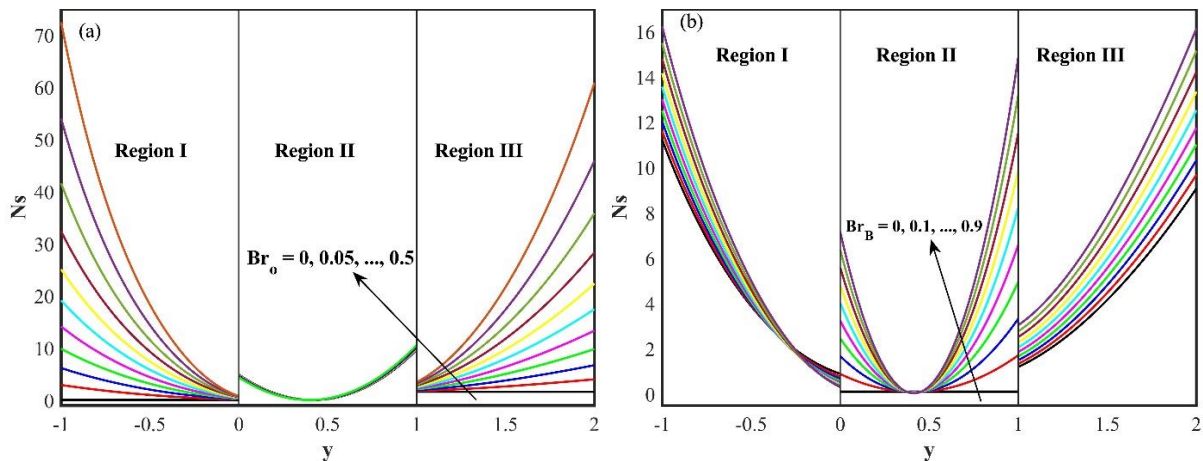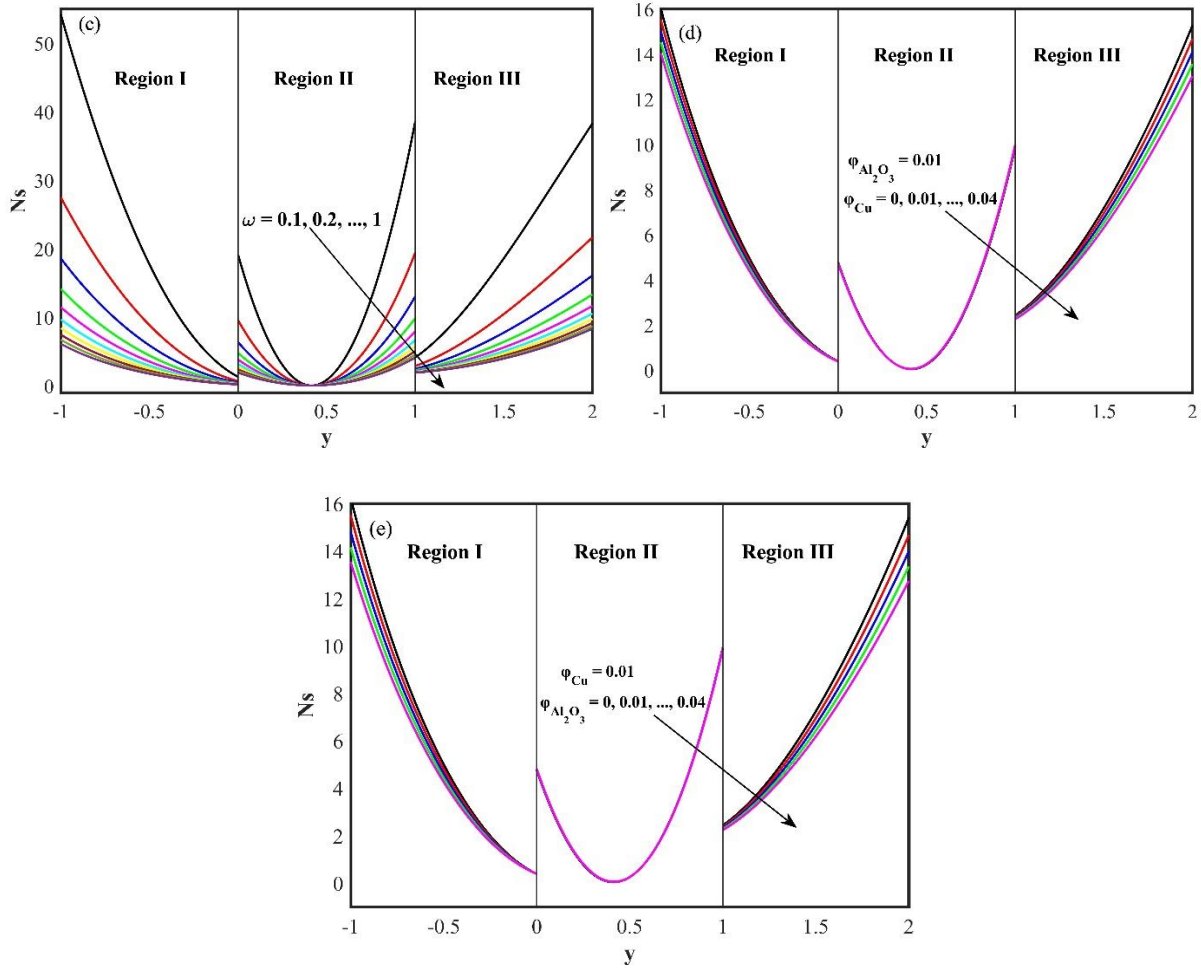
FIG. 12. Influence of (a) Br_o, (b) Br_B, (c) ω, (d) φ_{Cu}, and (e) $\varphi_{Al_2O_3}$ on entropy generation number (Ns).

Fig. 12 (a), (b), (c), (d), and (e) present the effects of the Brinkman number for oil (Br_o), Brinkman number for BVBF (Br_B), characteristic temperature ratio (ω) and NVF (φ_{Cu} & $\varphi_{Al_2O_3}$) on Ns. In Figs. 12 (a) & (b), there is an improvement in EG number with the increase in the values of both Brinkman numbers (Br_B and Br_o). Physically, the Brinkman number reflects the heat generation source that generates heat in the liquid layers. In Fig. 12 (c), an increase in the characteristic temperature ratio reduces the entropy generation rate. The temperature at the wall is greater than the temperature difference and the characteristic temperature ratio is defined as $\omega = \frac{T_{w1} - T_{w2}}{T_{w2}}$. Since the temperature at the wall is inversely proportional to the characteristic temperature ratio, a decrement is observed. In Fig. 12 (d) and (e), as values of NVF (φ_{Cu} & $\varphi_{Al_2O_3}$) upsurges the entropy generation number decreases. The temperature decreases as the values of NVF increase (as seen in Figs. 7 and 8) and this reduction in the temperature leads to a decline in the entropy generation.
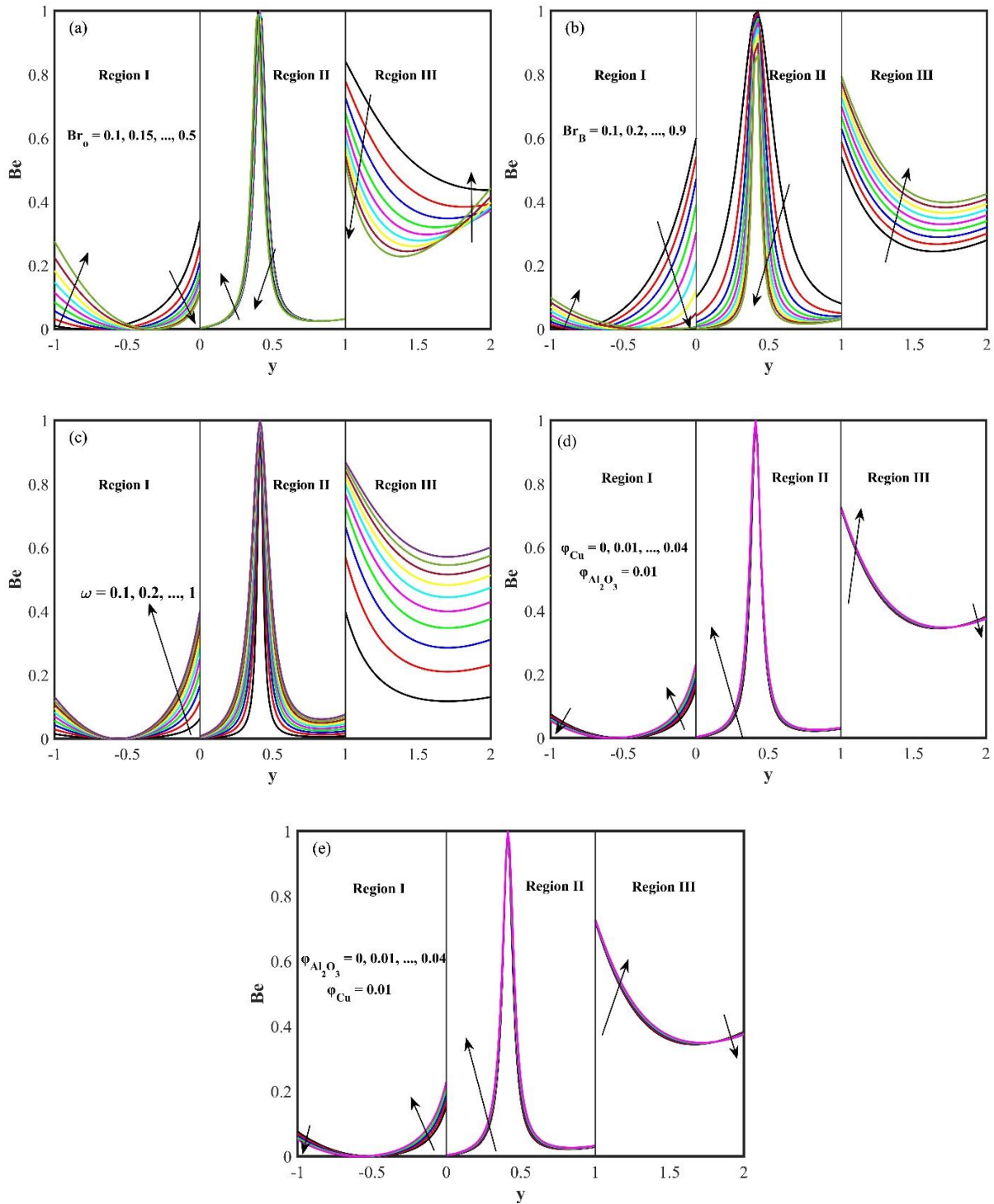
FIG. 13. Influence of (a) Br_o, (b) Br_B, (c) ω, (d) φ_{Cu}, and (e) $\varphi_{Al_2O_3}$ on entropy generation number (Be).

Fig. 13 (a), (b), (c), (d), and (e) present the effects of Brinkman number for oil (Br_o), Brinkman number for BVBF (Br_B), characteristic temperature ratio (ω) and NVF (φ_{Cu} & $\varphi_{Al_2O_3}$) on the Bejan number (Be). In Fig. 13 (a), Bejan number shows a dual behavior for increasing values of the Brinkman number for oil (Br_o) in all regions. While the Bejan

number in region II did not vary significantly as compared to other regions. In Fig. 13 (b), an increase in the values of the Brinkman number for BVBF, the Bejan number in region II decreases whereas it blows up to a certain value within regions II. In region III, the Bejan number upsurges with Br_B. But a dual nature in the Bejan number is observed due to upsurge in the values of Br_B in region I. In Fig. 13 (c), the Bejan number increases with increasing values of characteristic temperature ratio in all regions. This is due to the positive relationship between the Bejan number and the characteristic temperature ratio. But the impact of temperature ratio on Bejan number is more evident in region III than in other regions. Fig. 13 (d) and (e) show that the impact of φ_{Cu} & $\varphi_{Al_2O_3}$ is qualitatively similar on the Bejan number. The Bejan number of BVBF layer increases with a rise in the NVF, while the Bejan number of hybrid nanofluid layers demonstrate dual behavior due to the increase in NVF.

TABLE V. Nusselt number (Nu_l & Nu_r) and skin friction coefficient (Cf_l & Cf_r) values of left and right walls for various parameters.

		Nu_l	Nu_r	Cf_l	Cf_r
	0.2	-1.588357	-3.963059	5.438501	-4.294240
Qc	0.3	-1.819452	-4.128500	5.743178	-4.442757
	0.4	-2.091108	-4.323586	6.076461	-4.612194
	0.5	-0.478417	-3.112339	3.554965	-3.274945
λ	1.5	-1.127828	-3.612970	4.759444	-3.909596
	2.5	-2.190052	-4.419868	6.202490	-4.752431
	0.01	-1.923605	-4.221013	5.534063	-4.406279
φ	0.03	-1.712092	-4.056618	5.490634	-4.341121
	0.05	-1.514074	-3.906256	5.451038	-4.279756
	1.5	-1.873607	-3.794554	5.594763	-4.431930
Rd	2	-1.588357	-3.963059	5.438501	-4.294240
	2.5	-1.335672	-4.156752	5.330622	-4.198905
	0.5	-1.843489	-4.197581	5.546123	-4.367583
Br_B	0.7	-1.406815	-3.796375	5.361347	-4.243688
	0.9	-1.164755	-3.574478	5.257468	-4.178744

Table V presents the numeric values of the Nusselt number (Nu_l & Nu_r) and skin friction coefficient (Cf_l & Cf_r) for different values of Qc, λ, φ, Rd and γ. The Nusselt number (Nu_l & Nu_r) increases with Brinkman number for BVBF (Br_B) and NVF whereas decreases for the quadratic convection parameter and mixed convection parameter at both walls. The Nusselt number at the left wall increases and decreases at the right wall for the radiation parameter. The skin friction coefficient at the left wall increases for the quadratic convection parameter and mixed convection parameter whereas decreases for the radiation parameter, and

Brinkman number for BVBF and NVF. The skin friction coefficient at the right wall increases for the radiation parameter, Brinkman number for BVBF and NVF whereas decreases for the quadratic convection parameter and mixed convection parameter. After a detailed discussion of the results obtained in the study, the major conclusions are listed in the next section.

V. CONCLUSIONS

From this analysis, we conclude the following:

- The nonlinear density-temperature variation leads to a significant improvement in the magnitude of the velocity and temperature profiles due to the increased buoyancy force. As a result, the drag force on the walls is condensed. Therefore, the nonlinear variation in density with temperature cannot be ignored if the temperature difference in the system is relatively large.

- The velocity and temperature distributions have enhanced due to larger Brinkman numbers. While the Brinkman number for BVBF has a more evident impact in region II among all regions.

- The shear stress on the right wall is reduced due to nonlinear convection and mixed convection. While this trend is contradictory for left wall shear stress.

- The drag force on the slab gets enhanced by increasing the volume of nanoparticles.

- The dragging effect due to the continuance of interfacial conditions is observed. That is, the BVBF parameter is only present in region II but the effect is also visible in regions I and III as well. Similarly, the hybrid nanoliquid is present in regions I and III, but the effect of NVF is visible in region II.

- By increasing the volume of nanoparticles from 1% to 3%, the heat transport improved by 11% on the left wall, whereas the heat transport on the right wall improved by 3.9%.

- For the variation of all parameters following relations are valid: $Nu_l > Nu_r$ and $Cf_l > Cf_r$.

- The Brinkman numbers increase the entropy generation rate while the characteristic temperature ratio and NVF produce a decrease in the entropy generation rate.

- An increase in the Brinkman numbers leads to a reduction in the Bejan number.

- In the multilayer flow problem, the Bejan number decreases for the BVBF parameter in region II and increases in regions I and III due to the irreversibility of fluid friction. Similarly, near the walls, there is a decrease in the Bejan number and an increasing Bejan number can be found elsewhere when NVF has increasing values.

- The comparison of the results obtained with the Differential Transformation Method and the bvp5c method found excellent agreement and therefore established the accuracy of the DTM. Therefore, DTM can be successfully applied to handle multipoint nonlinear boundary value problems.

DECLARATION OF COMPETING INTEREST

The authors declare that they have no competing interests.

DATA AVAILABILITY

The data that support the findings of this study are available from the corresponding author upon reasonable request.

ACKNOWLEDGMENT

REFERENCES

[1]R.P. Chhabra, and J.F. Richardson, Butterworth-Heinemann (2011).

[2]E. C. Bingham, Bull Bur Stand, **13**, 309 (1916).

[3]I.A. Frigaard, K.G. Paso, and P.R. de Souza Mendes, Rheologica Acta, **56**, 259 (2017).

[4]M. Nakamura, and T. Sawada, Journal of non-newtonian fluid mechanics, **22**, 191 (1987).

[5]N. Casson, Rheol. of disperse sys., 84 (1959).

[6]B.S. Dandapat, S.K. Singh, and S. Maity, International Journal of Mechanical Sciences, **130**, 367 (2017).

[7]T. Hayat, S. A. Shehzad and A. Alsaedi, Appl. Math. Mech. **33**, 1301 (2012).

[8]C. R. Reddy, C. V. Rao and O. Surender, Procedia Eng. 127, 1219 (2015).

[9]M. Kumar, and P.K. Mondal, Physics of Fluids, 33, 093113. (2021).

[10]I. A. Frigaard, and R. J. Poole, Physics of Fluids, 33, 129101 (2021).

[11]S. U. S. Choi and J. A. Eastman, The Proc. of the 1995 ASME Int. Mech. Eng. Congress Expo. **66**, 99 (1995).

[12]K. Khanafer, K. Vafai and M. Lightstone, Int. J. Heat Mass Transf. **46**, 3639 (2003).

[13]S. Suresh, K. Venkitaraj, P. Selvakumar and M. Chandrasekar, Exp. Therm. Fluid Sci. **38**, 54 (2012).

[14]M. Shruthy and B. Mahanthesh, J. Nanofluids **8**, 222 (2019).

[15]E. K. Ghiasi and R. Saleh, Eng. Appl. Sci. Lett. **2**, 21 (2019).

[16]Y.Ma and Z. Yang, Physics of Fluids, **32**, 012009 (2020).

[17]T.S. Kumar, Partial Differential Equations in Applied Mathematics, **4**, 100070 (2021).

[18]I. Waini, A. Ishak, and I. Pop, International Communications in Heat and Mass Transfer, **130**, 105804 (2022).

[19]N.C. Roy, and I. Pop, Physics of Fluids, **34**, 072005 (2022).

[20]H. Xu, Applied Mathematics and Mechanics, **43** 113 (2022).

[21]B. A. Packham and R. Shall, Math. Proc. Camb. Philos. Soc. **69**, 443 (1971).

[22]J. C. Umavathi and M. S. Malashetty, Int. J. Non Linear Mech. **40**, 91 (2005).

[23]K. Vajravelu, K. V. Prasad and S. Abbasbandy, Appl. Math. Mech. **34**, 177 (2013).

[24]B. Li, W. Zhang, L. Zhu and L. Zheng, Powder Technol. **310**, 351 (2017).

[25]R. Sarma, M. Jain and P.K. Mondal, Physics of Fluids, **29**, 103102 (2017).

[26]J. C. Umavathi and O. A. B*ég*, Int. J. Heat Mass Transf. **154**, 119613 (2020).

[27]S. L. Goren, Chem. Eng. Sci. **21**, 515 (1966).

[28]K. Vajravelu and K. S. Sastri, Int. J. Heat Mass Transf. **20**, 655 (1977).

[29]K. Vajravelu, J. R. Cannon, J. Leto, R. Semmoum, S. Nathan, M. Draper and D. Hammock, J. Math. Anal. Appl. **277**, 609 (2003).

[30]M. K. Partha, Appl. Math. Mech. **31**, 565 (2010).

[31]S. Shaw, P. K. Kameswaran and P. Sibanda, Bound. Value Probl. **55**, 1295 (2016).

[32]P. Naveen and C. RamReddy, Int. J. Adv. Trends Comp. Appl. (2019).

[33]P. M. Patil and M. Kulkarni, Rev. mex. de fís. **66**, 153 (2020).

[34]B. K. Jha and G. Samaila, Proc. Inst. Mech. Eng. Part E: J. Process Mech. Eng. (2021).

[35]B. Mahanthesh, Math. Fluid Mech., 13 (2021).

[36]A. Bejan, J. Heat Transfer, **101,** 718 (1979).

[37]A. Bejan, CRC Press, Boca Raton, NY (1996).

[38]J.R. Murthy and J. Srinivas, International Journal of Heat and Mass Transfer, **65**, 254 (2013).

[39]V. Bianco, O. Manca, and S. Nardini, Energy Conversion and Management, **77,** 306 (2014).

[40]K.Y. Leong, and H.C. Ong, International Communications in Heat and Mass Transfer, **57**, 72 (2014).

[41]V. Anand, Energy, **93**, 154 (2015).

[42]K. Ting, A.K. Mozumder, and P.K. Das, Physics of Fluids, **31**, 093602 (2019).

[43]J. K. Zhou, Huazhong University Press, Wuhan (1986).

[44]J. P. Kumar, J. C. Umavathi and J. Sharadkumar, Int. J. Eng. Res. Technol. **2**, 1117 (2013).

[45]J. C. Umavathi, J. P. Kumar and M. A. Sheremet, Phys. A:Stat. Mech. Appl. **465**, 195 (2017).

[46]A. Rajeev and B. Mahanthesh, Heat Transf. **50**, 4309 (2021).

[47]J. Kierzenka and L. F. Shampine, ACM Trans. Math. Softw. **27,** 299 (2001).

Appendix A: Analytical solution for a special case

The analytical solution of the equations (34)-(40) in the absence of viscous dissipation are given below:

Region I

$$u_1 = -(g_5 E_1^2)y^4 - (g_6 E_1 + g_7 E_1 E_2)y^3 - (g_8 E_2 + g_9 E_2^2 + g_{10})y^2 - E_3 y - E_4,$$

$$\theta_1 = \frac{E_1 y + E_2}{g_1},$$

Region II

$$u_2 = -(g_{15} E_5^2)y^4 - (g_{16} E_5 + g_{17} E_5 E_6)y^3 - (g_{18} E_6 + g_{19} E_6^2 + g_{20})y^2 - E_7 y - E_8,$$

$$\theta_1 = \frac{E_5 y + E_6}{g_{11}},$$

Region III

$$u_1 = -(g_5 E_9^2)y^4 - (g_6 E_9 + g_7 E_9 E_{10})y^3 - (g_8 E_{10} + g_9 E_{10}^2 + g_{10})y^2 - E_{11} y - E_{12},$$

$$\theta_1 = \frac{E_9 y + E_{10}}{g_1},$$

In the above expressions, the following constants g_1-g_{20}, E_1-E_{12} and N_1-N_{13} are used.

$$E_1 = E_2 - g_1; \quad E_2 = N_1 E_6; \quad E_3 = -g_6 E_1 + g_8 E_2 + E_4 + N_6; \quad E_4 = E_8$$

$$E_5 = N_2 E_1; \, E_6 = \frac{E_9 + E_{10}}{N_1} - E_5; \, E_7 = N_3 E_3;$$

$$E_8 = -g_{16} E_5 - g_{18} E_6 - E_7 + g_6 E_9 + g_8 E_{10} + E_{11} + E_{12} + N_9$$

$$E_9 = \frac{E_5}{N_2}; \, E_{10} = -2E_9; \, E_{11} = \frac{1}{N_3}(3g_{16} E_5 + 2g_{18} E_6 + E_7) - 3g_6 E_9 - 2g_8 E_{10} + N_{12};$$

$$E_{12} = -8g_6 E_9 - 4g_8 E_{10} - 2E_{11} - N_{13}; \, g_1 = D + Rd; \, g_2 = \frac{\lambda B}{A g_1}; \, g_3 = \frac{\lambda C Qc}{A g_1^2};$$

$$g_4 = \frac{P}{A}; \, g_5 = \frac{g_3}{12}; \, g_6 = \frac{g_2}{6}; \, g_7 = \frac{g_3}{3}; \, g_8 = \frac{g_2}{2}; \, g_9 = \frac{g_3}{2}; \, g_{10} = \frac{g_4}{2}; \, g_{11} = 1 + f_k Rd;$$

$$g_{12} = \frac{f_v f_r f_b \lambda}{\left(1 + \frac{1}{\gamma}\right) g_{11}}; \, g_{13} = \frac{f_v f_r f_d \lambda Qc}{\left(1 + \frac{1}{\gamma}\right) g_{11}^2}; \, g_{14} = \frac{f_v P}{\left(1 + \frac{1}{\gamma}\right)}; \, g_{15} = \frac{g_{13}}{12}; \, g_{16} = \frac{g_{12}}{6}; \, g_{17} = \frac{g_{13}}{3};$$

$$g_{18} = \frac{g_{12}}{2}; \, g_{19} = \frac{g_{13}}{2}; \, g_{20} = \frac{g_{14}}{2}; \, N_1 = \frac{g_1}{g_{11}}; \, N_2 = \frac{D f_k}{N_1}; \, N_3 = \frac{A f_v}{\left(1 + \frac{1}{\gamma}\right)}; \, N_4 = g_{10} - g_{20};$$

$$N_5 = \frac{2g_{20}}{N_3} - 2g_{10}; \, N_6 = g_5 E_1^2 - g_7 E_1 E_2 + g_9 E_2^2 + g_{10}; \, N_7 = g_{15} E_5^2 + g_{17} E_5 E_6 + g_{19} E_6^2;$$

$$N_8 = g_5 E_9^2 + g_7 E_9 E_{10} + g_9 E_{10}^2; \, N_9 = N_4 - N_7 + N_8; \, N_{10} = \frac{1}{N_3}(4g_{15} E_5^2 + 3g_{17} E_5 E_6 + 2g_{19} E_6^2); \, N_{11} = 4g_5 E_9^2 + 3g_7 E_9 E_{10} + 2g_9 E_{10}^2; \, N_{12} = N_5 + N_{10} - N_{11};$$

$$N_{13} = 16g_5 E_9^2 + 8g_7 E_9 E_{10} + 4g_9 E_{10}^2 + 4g_{10}.$$

Appendix B: Nomenclature

a_R	Rosseland mean absorption factor (m^{-1})	λ	Mixed convection parameter
A, B, C, D	Constants	μ	Dynamic viscosity ($kgm^{-1}s^{-1}$)
Br	Brinkman number	ν	Kinematic viscosity (m^2s^{-1})
C_p	Heat capacity ($Jkg^{-1}K^{-1}$)	θ	Dimensionless temperature
C_f	Skin friction factor	Θ	Transformed temperature notation of DTM
e_b	Blackbody emissive power	ρ	Density (kgm^{-3})
f_b & f_d	Ratio of coefficient of thermal expansion	τ_{ij}	Cauchy stress tensor
f_k	Ratio of thermal conductivity	τ, η	Transformations
f_r	Ratio of density	ω	Characteristic temperature ratio
f_v	Ratio of viscosity	π	Product of deformation tensor
g	Acceleration due to gravity (ms^{-2})	π_c	Critical value
Gr	Grashof number	φ	Total nanoparticle volume fraction
h	Length scale (m)	Φ	Viscous dissipation
k	Thermal conductivity ($Wm^{-1}K^{-1}$)	σ_{SB}	Stefan-Boltzmann constant $(Wm^{-2}K^{-4})$
Nu	Nusselt number	**Subscripts**	
p	Pressure ($kgm^{-1}s^{-2}$)	B	BVBF
P	Pressure gradient parameter	o	oil
p_y	Yield stress	hno	Hybrid nano oil
q	Conduction heat flux	l	left wall
q_r	Radiative heat flux	r	right wall
Qc	Quadratic convection parameter	Cu	Copper
Rd	Thermal radiation parameter	Al_2O_3	Aluminium oxide
Re	Reynolds number	$i(1,2,3)$	Regions I, II, III
t	Time (s)	**Abbreviations**	
T	Temperature (K)	Be	Bejan number
T_w	Temperature (K) at walls	$BVBF$	Bi-viscous Bingham fluid
$\bar{u}$	Average velocity (ms^{-1})	DTM	Differential Transform Method
u	Dimensionless velocity	Eg	Entropy generation
U	Velocity velocity (ms^{-1})	Eg_o	Characteristic entropy generation
$\mathcal{U}$	Transformed velocity notation of DTM	FFI	Fluid friction irreversibility
X, Y	Cartesian coordinates (m)	HTI	Heat transfer irreversibility
Greek symbols		LBA	Linear Boussinesq approximation
α, ε	Unknown constants	Ns	Local entropy generation number
β & β^*	Thermal expansion coefficient (K^{-1})	NVF	Nanoparticle volume fraction
γ	BVBF parameter	QBA	Quadratic Boussinesq approximation